Fisheries and Oceans Canada | Pêches et Océans Canada
Ecosystems and Oceans Science | Sciences des écosystèmes et des océans

Canadian Science Advisory Secretariat (CSAS)

Research Document 2022/075

Newfoundland and Labrador Region

Optical, Chemical, and Biological Oceanographic Conditions on the Newfoundland and Labrador Shelf during 2018

G. Maillet, D. Bélanger, G. Doyle, A. Robar, S. Rastin, D. Ramsay and P. Pepin

Science Branch
Fisheries and Oceans Canada
PO Box 5667
St. John's, Newfoundland and Labrador A1C 5X1

December 2022

Canada

Foreword

This series documents the scientific basis for the evaluation of aquatic resources and ecosystems in Canada. As such, it addresses the issues of the day in the time frames required and the documents it contains are not intended as definitive statements on the subjects addressed but rather as progress reports on ongoing investigations.

Published by:

Fisheries and Oceans Canada
Canadian Science Advisory Secretariat
200 Kent Street
Ottawa ON K1A 0E6

http://www.dfo-mpo.gc.ca/csas-sccs/
csas-sccs@dfo-mpo.gc.ca

ISSN 1919-5044
ISBN 978-0-660-46097-0 Cat. No. Fs70-5/2022-075E-PDF

Correct citation for this publication:

Maillet, G., Bélanger, D., Doyle, G., Robar, A., Rastin, S., Ramsay, D. and Pepin, P. 2022. Optical, Chemical, and Biological Oceanographic Conditions on the Newfoundland and Labrador Shelf during 2018. DFO Can. Sci. Advis. Sec. Res. Doc. 2022/075. viii + 53 p.

Aussi disponible en français :

Maillet, G., Bélanger, D., Doyle, G., Robar, A., Rastin, S., Ramsay, D. et Pepin, P. 2022. Conditions océanographiques optiques, chimiques et biologiques sur le plateau continental de Terre-Neuve-et-Labrador en 2018. Secr. can. des avis sci. du MPO. Doc. de rech. 2022/075. ix + 56 p.

TABLE OF CONTENTS

LIST OF TABLES

LIST OF FIGURES

ABSTRACT

Ocean nutrients and plankton conditions on the Grand Bank and Newfoundland and Labrador shelves in 2018 were assessed and compared to long-term average conditions in the region to highlight relationships between biogeochemical oceanographic conditions and marine primary (phytoplankton) and secondary (zooplankton) production. Overall, optical and chlorophyll *a* indices indicated above normal phytoplankton biomass in April-May 2018 at the high frequency sampling station (S27). Phytoplankton production indices during the remainder of the year were consistent with normal conditions. Silicate and nitrate profiles in spring indicated uptake to depths nearly two-fold deeper compared to the climatology and implies that a portion of primary production occurred deeper within the euphotic layer. The annual chlorophyll anomalies along the cross-shelf sections also indicated higher phytoplankton production in 2018 which contrasts with lower levels observed back to the early 2010's. Although broad-scale ocean colour imagery during spring 2018 was consistent with Atlantic Zone Monitoring Program (AZMP) in situ observations, bloom indices at smaller regional scales indicated limited bloom amplitude and magnitude. The general trend of increasing zooplankton abundance observed on the Grand Bank since the start of the monitoring program continued in 2018. The abundance of large, energy-rich *Calanus finmarchicus* copepods was mainly near normal on the Grand Bank and the NL shelves in 2018 after 4 years of low abundance. The abundance of the small copepod taxa *Pseudocalanus* spp. and *Oithona* spp. was back to near normal levels after 3–4 years of high abundances with the exception of the southeastern Grand Bank where abundances remained above normal. The abundance of non-copepod zooplankton continued to be above normal across the region for a 6th consecutive year, reaching either highest or second highest levels of the time series at S27 and on all oceanographic sections. The production cycles of *C. finmarchicus* and *Pseudocalanus* spp. at S27 were delayed ~1 month in 2018 with evidence of the production of a second generation. Large (>1 mm) planktonic organisms were mainly responsible for the increased zooplankton biomass in all oceanographic cross-shelf sections. The biomass of small zooplankton (<1 mm) showed negative anomalies across the region, continuing a trend that started more than a decade ago. The relative abundance of near-surface phyto- and zooplankton taxa based on the Continuous Plankton Recorder (CPR) survey indicated enhanced levels of small copepods and acid-sensitive plankton on the northern Grand Bank. Changes in ocean acidification and carbonate chemistry indicate seasonal variations in pH and in saturation horizons of aragonite and calcite. Ocean carbon measurements generally indicate that water masses are saturated in regard to carbonate ions but observations identified under-saturation of aragonite at intermediate and deeper bottom waters at certain stations. The overall pattern of variation among nutrients, phytoplankton biomass and zooplankton abundance highlights the relationship between the biogeochemical environment and the primary and secondary production. There are persistent signs of a shift in copepod community size structure characterized by a decline of large energy-rich calanoid copepods in favor of smaller copepod taxa. More research is needed to understand the underpinnings of these important changes in zooplankton community structure and their potential impact on the transfer of energy to higher trophic levels.

INTRODUCTION

The Atlantic Zone Monitoring Program (AZMP) was implemented in 1998 to enhance Fisheries and Oceans Canada's (DFO) capacity to understand, describe, and forecast the state of the marine ecosystem and to quantify the changes in the ocean physical, chemical and biological properties (Therriault et al. 1998). A critical element of the AZMP involves an observation program aimed at assessing the variability in nutrients, phytoplankton (microscopic primary producers) and zooplankton (drifting animals). The overall aim of the program is to identify fundamental relationships among elements of the planktonic ecosystem and establish how they respond to changes in environmental drivers. The AZMP derives its information on the state of the marine ecosystem from data collected at a network of sampling locations (high frequency sampling stations, cross-shelf sections, and multispecies trawl surveys) in four DFO regions (Quebec, Gulf, Maritimes, Newfoundland and Labrador [NL]) sampled at a frequency of twice-monthly to once-annually. Cross-shelf sections provide information about broad-scale environmental variability but are limited in their seasonal coverage. High frequency sampling stations complement the broad-scale sampling by providing more detailed information on annual changes in ocean properties. The location of the standard oceanographic cross-shelf sections and high frequency sampling station for the NL region occupied in 2018 is shown in Figure 1.

A description of the seasonal patterns in the distribution of phytoplankton and zooplankton provides important information about organisms that form the base of the marine food web. An understanding of the production cycles of plankton, and their interannual variability, is an essential part of an ecosystem approach to fisheries management. This report provides an assessment of the distribution and abundance of macronutrients and plankton on the NL Shelves highlighting the biogeochemical oceanographic conditions in 2018 in relation to long-term average conditions based on archived data. Because the availability of nitrogen and silicate is most often associated with limiting the growth of phytoplankton in the northwest Atlantic, more emphasis in this report is placed on variability in these macronutrient inventories. It complements similar reviews of the biological oceanographic conditions in the Gulf of St. Lawrence, the Scotian Shelf and Gulf of Maine as part of the AZMP (Yashayaev et al. 2014, Johnson et al. 2020, Blais et al. 2018). This report also complements ocean climate and physical oceanographic assessments of the Region (e.g., Cyr et al. 2020) and for the Northwest Atlantic shelf system as a whole (DFO 2019).

Variability in biological oceanographic conditions may be driven by physical properties of the water column and boundary conditions. Typically, the water masses characteristic of the Newfoundland Shelf are dominated by subpolar waters with a sub-surface temperature range below 0°C. Labrador slope water flows southward along the shelf edge and into the Flemish Pass; this water mass is generally warmer and saltier than the subpolar shelf waters. On average, bottom temperatures remain near 0°C over most of the northern Grand Bank but increase to above 0°C in southern regions and at depths below 200 m along the slopes of the banks. North of the Grand Bank, bottom temperatures are generally warmer except for the shallow inshore regions where they are mainly below 0°C. Throughout most of the year the cold, relatively fresh water overlying the shelf is separated from the warmer higher-density water of the continental slope region by a strong temperature and density front. This winter-formed water mass is referred to as the Cold Intermediate Layer (CIL) and is considered a reliable index of ocean climate conditions. In general, shelf water masses undergo seasonal modification in their properties as a result of the seasonal cycles of air-sea heat flux, wind-forced mixing and ice formation and melt, leading to intense vertical and horizontal gradients particularly along the frontal boundaries separating the shelf and slope water masses.

METHODS

To the extent possible, sample collection and processing conforms to established standard protocols (Mitchell et al. 2002). Non-standard measurements or derived variables are described below. The ecosystem production units (EPU) defined by the Northwest Atlantic Fisheries Organization (NAFO) are used in this report to refer to the different subregions of the Newfoundland Shelf waters (Figure 2).

SAMPLE COLLECTION

Three seasonal (spring, summer, fall) surveys were conducted along standard cross-shelf sections (Seal Island [SI], Bonavista Bay [BB], Flemish Cap [FC], and Southeast Grand Bank [SEGB]) in the NL region during 2018, in addition to occupations of the high frequency sampling coastal station (Station 27 [S27]) during AZMP missions and multispecies surveys (Table 1, Figure 1). Additional cross-shelf sections (Southwest St. Pierre Bank [SW-SPB], White Bay [WB], Makkovik Bank [MB] and Beachy Island [BI]) are occupied seasonally when time permits but are not reported in this document (Figure 1).

A total of 415 hydrographic stations occupations were performed in 2018. Seawater and plankton samples were collected at 220, and 231 stations respectively, including 25 occupations of the high frequency sampling station S27 between April and December 2018. Sampling at S27 and along the standard cross-shelf sections included a conductivity, temperature, depth (CTD) profile using CTD-Rosette mounted with a SBE-9plus (Sea-Bird Electronics) instrument equipped with dissolved oxygen, chlorophyll *a* fluorescence, photosynthetically active radiation (PAR), pH, coloured dissolved organic matter (CDOM) and transmissometer sensors. In the absence of a CTD profile, an expendable bathythermograph (XBT) was sometimes used.

Water samples were collected at standard depths of 5, 10, 20, 30, 40, 50, 75, 100, 150, 250, 500, and 1,000 m, as well as near bottom using Niskin bottles for salinity, oxygen, chlorophyll *a*, and nutrient analyses. In addition to the standard analyses for biological and chemical conditions, particulate organic carbon (POC) and nitrogen (PON), as well as carbonate (total alkalinity [TA] and total dissolved inorganic carbon [DIC]) are routinely collected at a subset of stations and depths to assess the formation of particulate matter and ocean acidification. Zooplankton samples were collected using a 75 cm diameter ring net (202 µm mesh Nitex) towed vertically from near the bottom (maximum tow depth of 1,000 m in deep offshore waters) to the surface at a speed of approximately 1 m s^{-1}. Samples were preserved in 4% buffered formaldehyde solution and analyzed according to the protocol outlined in Mitchell et al. (2002).

OPTICAL PROPERTIES

The optical properties of seawater (vertical attenuation coefficient [K_d], and euphotic depth [Z_{eu}]) were derived from in situ light extinction measurements using a rosette-mounted PAR meter. The downward vertical attenuation coefficient of PAR (K_{d_PAR}) was estimated as the slope of the linear regression of ln ($E_d[z]$) versus depth z (where $E_d(z)$ is the value of downward PAR irradiance at depth (z) in the depth interval from near surface to 50 m. Estimates of euphotic depth (ca. depth of 1% incident PAR) was computed using:

Z_{eu} (m) = 4.6 / K_{d_PAR}

When in situ PAR data were not available, a vertical attenuation coefficient based on chlorophyll *a* concentration (K_{d_chla}) was calculated using the equation:

K_{d_chla} (m^{-1}) = 0.027 m^{-1} + 0.015 m^{-1} + B(z) * 0.04 m^{-1} (Platt et al. 1988)

where B(z) is the concentration of chlorophyll *a* in mg m^{-3} and where additional coefficients are related to the components of pure seawater and dissolved substances. The euphotic depth is then calculated by substituting the average value of K_{d_chla} for the depth interval 0–50 m to K_{d_PAR}.

VERTICALLY INTEGRATED VARIABLES

Integrated chlorophyll (0–100 m) and nutrient (0–50 m and 50–150 m) inventories were calculated using trapezoidal numerical integration. When the maximum depth at a given station is shallower than the lower depth limits noted above, the inventories are calculated by setting the lower integration limit to the maximum depth at that station. Data at the surface (0 m) is taken as the closest near-surface sampled value. Data at the lower depth is taken as:

1. the interpolated value when sampling is below the lower integration limit; or
2. the closest deep water sampled value when sampling is shallower than the lower integration limit.

ANNUAL ANOMALIES SCORECARDS

Scorecards of key indices, based on standardized anomalies, represent physical, chemical, and biological observations in a compact format. Annual estimates of inventories of nutrients, chlorophyll, and abundance of key zooplankton taxa along each of the four cross-shelf sections and at the high frequency sampling station are based on general linear models of the form

$$Density = \alpha + \beta_{YEAR} + \delta_{STATION} + \gamma_{SEASON} + \varepsilon$$

for the cross-shelf sections where *Density* is in units of m^{-2}, α is the intercept, ε is the error, and β, δ, and γ are the categorical effects of year, station location, and season, respectively, and of the form

$$Density = \alpha + \beta_{YEAR} + \delta_{MONTH} + \varepsilon$$

for the high frequency sampling station (Station 27) where β and δ are the categorical effects for year and month, respectively. Density is log-transformed (ln [*Density*]) to normalize the skewed distribution of the observations. In the case of zooplankton, one (1) is added to the density (ln [*Density* + 1]) to include observations where density equals zero. Values for the optical properties of seawater were not transformed. Models least square means based on type III sums of squares are used as estimates of annual means. Annual anomalies are calculated as the deviation of an individual year from the mean of the annual estimates over the standard climatology: 1998–2015 for satellite ocean colour data, and 1999–2015 for nutrients, chlorophyll, and zooplankton inventories. Anomalies are expressed as standardized quantities (i.e., by dividing by the standard deviation of the annual means over the climatology). Large departures from long-term average (climatology) conditions could be indicative of shifts in the dominant oceanographic regime or ecosystem processes.

SATELLITE REMOTE SENSING OF OCEAN COLOUR

Near-surface phytoplankton biomass was estimated from ocean colour satellite data collected by the Sea-viewing Wide Field-of-view Sensor (SeaWiFS) launched by the National Aeronautics and Space Administration (NASA) in September 1997, the Moderate Resolution Imaging Spectroradiometer (MODIS) “Aqua” sensor launched by NASA in July 2002, and the Visible-Infrared Imager Radiometer Suite (VIIRS) sensor launched by NASA and the National Oceanic and Atmospheric Administration (NOAA) in October 2011. Here, we combine ocean SeaWIFS composite data from 1998 to 2007, MODIS data from 2008 to 2011, and VIIRS data from 2012

to 2018 to construct surface chlorophyll time series in selected subregions in the NL region (Figure 3). The OCx (x = 4, 3M and 3V for SeaWIFS, MODIS and VIIRS, respectively) band-ratio algorithms are used to derive chlorophyll concentration from remote sensing reflectance as described in O'Reilly et al. (1998) with coefficients of the algorithms for each sensors accessible on NASA's OceanColor Web chlorophyll-*a* website. Basic statistics (mean, standard deviation) are extracted from semi-monthly composite images to create visualization products of the annual cycle and the interannual variability in surface chlorophyll concentration. These products are available on the Operational Remote Sensing section of the Bedford Institute of Oceanography webpage. Weekly (8-day composite) satellite data were used to describe spring bloom phenology based on four metrics computed using a shifted Gaussian function of time model as described in Zhai et al. (2011):

- start date (day of year),
- cycle duration (days),
- magnitude (the integral of chlorophyll concentration under the Gaussian curve), and
- amplitude (maximum minus the background chlorophyll concentration).

OBSERVATIONS

OPTICAL PROPERTIES

High frequency sampling station

Optical indices (i.e., attenuation coefficient and euphotic depth) generally track the dynamics of the phytoplankton production cycle. Generally, the attenuation of PAR gradually increases over the winter, peaks in April, rapidly declines through June, and remains relatively stable throughout summer and fall (Figure 4A). In 2018, attenuation coefficients in April and May were well above the climatology, indicating a more intense spring bloom compared to normal. Vertical attenuation returned to near normal through the summer. The less intense fall bloom is normally difficult to observe based on the seasonal changes in optical indices but, was noticeably higher in October 2018 (Figure 4A). Annual mean coefficients indicated a variable trend with a record high in 2018 (Figure 4B). The euphotic depth (depth at 1% incident PAR) generally varies seasonally between 35 and 85 m (Figure 4C). It starts to decrease in January to a minimum in April during the spring bloom, then rapidly increases to a maximum in June, and remains relatively stable during summer and fall. Euphotic depth in April 2018 was shallower by nearly two-fold compared to the climatology. Values observed during the summer were generally near the climatology. Light penetration was also lower than average in September and October 2018 suggesting higher fall production (Figure 4C). The annual mean euphotic depth generally trended to deeper depths from 2000 until 2014 followed by a marked decrease to a record low value in 2017 (Figure 4D). Mean euphotic depth in 2018 was the second lowest of the time series.

In 2018, spring integrated chlorophyll inventories were ~600 and 300 mg m^{-2} in April and May, respectively, which was well above climatology (Figure 4E). The above-normal attenuation coefficient in September, and the below-normal euphotic depths in September and October suggested a relatively intense fall bloom in 2018. Chlorophyll inventories, however, were consistent with normal conditions during the same period. While the spring bloom develops across most of the euphotic depth, the fall bloom generally occurs closer to the surface. The near-surface production of the fall becomes slightly diluted when integrated across a 100 m water column, which may explain why our integrated chlorophyll inventories fail to capture the

fall bloom. Annual mean inventories showed an overall decline from ~250 mg m^{-2} at the start of the series, to a minimum of ~40 mg m^{-2} in 2016, before increasing to ~170 mg m^{-2} in 2018; the second-highest value of the time series (Figure 4F).

NUTRIENTS AND CHLOROPHYLL INVENTORIES

High frequency sampling station

The vertical distributions of inorganic nutrients at S27 show strong seasonal co-variation of nitrate, silicate and phosphate. The inventories of nutrients are influenced by seasonal biological processes operating throughout the upper water column and by deep water microbial recycling. In addition, determining the initiation of nutrient uptake is dependent on sampling effort, and the frequency of observations is limited in winter and early spring compared to other times of the year.

Dominant features of the annual production cycle were inferred from comparison of climatological vertical structure and monthly variability in the concentration of nutrients and chlorophyll. The distribution of all macronutrients show strong vertical stratification throughout the year (Figure 5A-F). The climatology for phosphate indicates uptake beginning in early March with increasing drawdown through the summer months. Concentrations of phosphate then begin to increase in August, reaching a maximum in January. Vertical uptake of phosphate is generally limited to the upper 50 m of the water column. The uptake in phosphate observed in 2018 was more extensive than normal. A first drawdown reaching in excess of 100 m occurred in April-May, substantially earlier compared to normal (Figure 5B). A second drawdown was also apparent in late summer 2018, but limited to the upper 50 m. In addition, deep phosphate concentrations were slightly higher in 2018 compared to the climatology during the fall when microbial recycling of organic matter increases. Increased bottom concentrations in all macronutrients during the summer and fall periods in 2018 were also noted, compared to the climatology.

The climatology for silicate and nitrate indicates uptake also begins in March with extensive drawdown of nitrate and silicate to near limiting (i.e., approaching zero) concentrations until the late fall in the upper 50–75 m of the water column (Figure 5C, E). Silicate generally replenishes more rapidly than nitrate with concentrations approaching ~4 mmol m^{-3} in late fall compared to ~2 mmol m^{-3} for nitrate. The drawdown pattern for silicate and nitrate in 2018 was similar to that of phosphate but with earlier and more extensive uptake during spring with limiting concentrations down to depths in excess of 100 m (Figure 5D, F). Based on the available data, nitrate appears to be the rate limiting nutrient compared to either phosphate or silicate, particularly during the periods of highest production observed during the spring and fall periods.

The vertical distribution of chlorophyll biomass is generally consistent with the dynamics of nutrients. The climatology shows increasing concentrations of chlorophyll above background levels beginning in late February-early March and peaking at ~4 mg m^{-3} in April during the spring bloom in the upper 50 m (Figure 6A). The spring production cycle normally extends from February-May. Phytoplankton biomass declines rapidly to background levels during early summer, increasing again to concentrations of ~1–2 mg m^{-3} confined to the upper 40 m during the fall bloom (Figure 6A). In 2018, concentrations of chlorophyll reached in excess of 5 mg m^{-3} and higher levels were observed deeper than normal (Figure 6B). However, the fall bloom was weaker than normal based on measured chlorophyll concentrations but similar in timing in 2018 compared to the climatology. Given the limited timing of the fall bloom, it is possible that the sampling program may have missed a portion of the production cycle.

A summary of monthly integrated inventories of macronutrients from S27 during the reference period indicate high (~150–200 mmol m^{-2}) levels of silicate and nitrate are maintained in the upper (0–50 m) water column from January through March (Figure 7A, B). Thereafter, rapid declines are observed in both of these nutrients within 1 month, followed by a smaller decline through the end of May. Rebuilding of the shallow inventories begins in early summer and progresses more rapidly in the fall, particularly in the case of silicate, to approach pre-winter conditions (Figure 7A, B). In 2018, no data were available during January through March, but both shallow inventories of these nutrients remained below normal until the fall when they approached and slightly surpassed the climatology (Figure 7A, B).

The deep (50–150 m) inventories vary between ~400 and 650 mmol m^{-2} seasonally with no distinct trend during the reference period. The minima in deep silicate and nitrate inventories occur in May and October respectively, while the inventory maxima for both nutrients is observed in August. Large reductions in deep silicate inventories in June, August and September 2018 were noted, compared to the climatology (Figure 7C, D). The mean seasonal inventories in deep nitrate were below normal throughout the year in 2018, although there was large uncertainty in these monthly means due to the limited number of observations.

Cross-shelf sections

Annual anomaly time series of shallow (0–50 m) and deep (50–150 m) inventories of nitrate and silicate along the different cross-shelf sections and at S27 were used to assess long-term trends across the NL region. In general, the nutrient inventories show short-term coherent trends along with high variability between positive and negative anomalies during the past two decades (Figure 8A-D). Shallow silicate inventories were highest during the early time series, and lowest between the late 2000's and early 2010's with a general negative trend over the series (Figure 8B). Shallow silicate and nitrate inventories showed similar variation trends with higher levels in the early 2000's and lower levels during the late 2000's through to 2018 (Figure 8A, B). Contrary to silicate, nitrate inventories in the upper layer have increased since 2015 along most sections, although conditions in 2018 were generally below normal.

Deep nitrate and silicate inventories followed similar variation patterns, shifting from mostly positive anomalies in the first half of the series to mostly near or below normal levels in the late 2000's (Figure 8C, D). The exception to this pattern was the negative silicate anomalies observed in 1999 and 2000 in nearly all ocean sections and S27 (Figure 8D). Deep nitrate inventories briefly increased to near or above normal in 2015–2017 before returning to below normal levels across the region in 2018 (Figure 8C). Chlorophyll inventories in the upper 100 m remained mostly near to above normal across sections and at S27 from the start of the monitoring program through 2010 (Figure 9). Thereafter, chlorophyll inventories decreased to below normal through until 2017. In 2018, chlorophyll inventories were near or above normal along all sections consistent with observations at S27. In general, the decline in the deep inventories of nitrate and silicate aligns with the low chlorophyll levels observed in the early to mid-2010's (Figure 9).

SATELLITE OCEAN COLOUR

Satellite ocean color data provides a broad-scale perspective of surface phytoplankton biomass over the whole of the Northwest Atlantic that is not possible for conventional vessel-based sampling. Satellite imagery supplements ship-based observations and provides seasonal coverage and a large-scale context to interpret survey data. The ocean colour imagery provides information about the timing and spatial extent of the spring and fall blooms but does not provide information of the dynamics that take place below the top few meters of the water

column. Subsurface information is obtained through in situ high frequency sampling at the S27 and seasonal oceanographic surveys.

Ocean colour anomaly maps over the Northwest Atlantic showed changes in the timing and intensity of the spring phytoplankton bloom in 2018. The early development of surface blooms started in late March and was largely confined to the northern Grand Bank and extended northwards to the Newfoundland Shelf (Figure 10). High concentrations of surface chlorophyll were observed in the southern Labrador Sea with lower levels on the Shelf waters. The anomaly map for this period showed extensive positive anomalies throughout the northern Grand Bank, and the Newfoundland and Labrador shelves including the Labrador Sea. Chlorophyll concentration on the southern Grand Bank was mostly near to slightly below normal during late March. By early April, surface chlorophyll concentrations intensified on the northern portion and slope waters of the Grand Bank, and the offshore areas of the Newfoundland Shelf. The extensive bloom observed in early April began to moderate two weeks later but remained above normal throughout the northern Grand Bank and slope waters of the Newfoundland Shelf. By early May, surface chlorophyll concentrations had reached high levels in the inshore areas of the Newfoundland Shelf and continued above normal along the slope waters of the northern Grand Bank. Anomaly maps indicated continued high levels of chlorophyll on the Newfoundland Shelf in late May while conditions on the Grand Bank were back to near normal levels (Figure 10).

We computed the spring bloom metrics (initiation, duration, amplitude and magnitude) for 11 subregions in the Northwest Atlantic (Figure 3). Data was insufficient in some of the northern areas to permit estimation of the different production metrics in certain years. The initiation of the spring bloom varies by latitude, ranging from late March on the southern Grand Bank to early June in northern Labrador. Blooms on the Flemish Cap/Pass are generally delayed by 10–15 days compared to the Grand Bank (Figure 11A). In 2018, the timing of bloom initiation was near normal on the Grand Bank but delayed on the Newfoundland and Labrador shelves (Figure 11A). Spring blooms typically last between 30 and 40 days, but can extend to up to nearly 3 months in northern Labrador due to the longer photoperiod and nutrient availability (Figure 11B). Overall, spring bloom duration has transitioned from longer than normal from 1998–2005, to shorter than normal from 2008 onwards across the region, with the exception of longer blooms on the Flemish Cap/Pass and the northeast Newfoundland Shelf in 2016 and 2017 (Figure 11B). Bloom duration on the Grand Bank in 2018 was mostly near normal, contrasting with the shorter blooms observed in the previous year (Figure 11B).

The amplitude of spring blooms typically varies between 1–3 mg m^{-3} among the subregions, but is generally highest on the Southeast Shoal (Figure 11C). Bloom amplitude was mostly below normal from 1998 to 2005. More intense blooms (positive anomalies) occurred between 2006 and 2015 without clear temporal or spatial patterns, except for 2006 and 2011 when high chlorophyll concentrations occurred throughout the NL region (Figure 11C). Bloom amplitude was mostly below normal across subregions in 2016–17. In 2018, bloom amplitude was mainly below normal on the Grand Bank and the Labrador Shelf, and above normal on the Flemish Cap/Pass and Newfoundland Shelf (Figure 11C).

Spring bloom production (magnitude) typically ranges between ~30 and 90 mg m^{-2} d^{-1} with no clear latitudinal patterns (Figure 11D). Similarly, no clear temporal or spatial trends were observed in spring bloom magnitude between 1998 and 2011, except for 2006 when above normal production occurred across the region (Figure 11D). Consistent with trends in bloom amplitude, a decline in magnitude is evident since 2012 with the exception of the markedly high production observed in 2014 in the Avalon Channel and southeast Shoal subregions (Figure 11D). Overall, spring production in the Hudson Strait, Flemish Cap, northeast, and southern Grand Bank is 1.2 to 2.7 times higher than any other subregion (Figure 11D).

The fall bloom is normally lower in amplitude and magnitude compared to the spring bloom but can cover extensive areas across the northwest Atlantic. Ocean colour imagery indicated surface concentrations of chlorophyll of 1–3 mg m^{-3} from the northern part and slope waters of the Grand Bank to Newfoundland Shelf waters further north in early September (Figure 12). The anomaly map for this period showed positive anomalies throughout the northern Grand Bank and Newfoundland and Labrador shelves on the order of ~2–3 mg m^{-3} above climatology (Figure 12). The fall bloom expanded on the Grand Bank during late September with above-normal surface concentrations across the region (Figure 12).

ZOOPLANKTON – HIGH FREQUENCY SAMPLING STATION (S27)

Community composition

Copepods typically dominate mesozooplankton abundance in marine ecosystems. At S27, copepods normally account for over 80% of total zooplankton abundance at any time of the year (Figure 13A). In 2018 the proportion copepods was lower than normal in most months from April to December (Figure 13B).

The copepod community is dominated by 11 taxa, with small cyclopoids *Oithona* spp. (mainly *O. atlantica* and *O. similis*) and calanoids *Pseudocalanus* spp. copepods accounting for 65–85% of total copepod abundance (Figure 13C). The large calanoid copepod *Calanus finmarchicus* is well represented from June-December while the even larger Arctic calanoids *C. glacialis* and *C. hyperboreus* are generally present from April-June (Figure 13C). The warmer-water adapted *Temora longicornis* is most represented from August to December (Figure 13C).

In 2018, the copepod assemblage at S27 was characterized by a decrease of ~10% in the proportion of *Oithona* spp. copepods compared to the climatology from June to December, and by an increase of up to 14% in the proportion of *Pseudocalanus* spp. during the same period (Figure 11C, D). The proportion of *T. longicornis* was ~10% lower than usual in August, and ~10% higher in October and November (Figure 13C, D). Monthly relative abundance of other copepod taxa generally did not depart from the climatology by more than 5% (Figure 13C, D).

Appendicularians (mainly *Fritillaria borealis* and *Oikipleura* spp.), gastropods, bivalves, and cladocerans typically dominate the non-copepod zooplankton community at S27. Gastropods are most represented in winter, appendicularians in spring and summer, cladocerans in summer, and bivalves in the fall (Figure 13E). In 2018, non-copepod representation was higher than normal, especially in June and August when their proportion increased by 17% and 21%, respectively, compared to the climatology (Figure 13B). The proportion of appendicularians was also markedly higher than normal from April through October, peaking at 96% in August (Figure 13F). As a result, relative abundances of gastropod and cladocerans were 19% and 23%, respectively, lower than the climatology during the summer months (Figure 13E, F).

Abundance

The abundance of large calanoids normally increases during the spring and peaks in June (Figure 14A-C). While the abundance of *C. finmarchicus* gradually decreases throughout summer and fall (Figure 14A), the abundance of *C. glacialis* and *C. hyperboreus* rapidly declines in July and August, respectively (Figure 14B, C). The abundance of *Pseudocalanus* spp. typically increases in late spring, remains high throughout summer, and declines in the fall (Figure 14D). The abundance of *Oithona* spp. is normally lowest in late spring and increases throughout summer and fall to peak in early winter (Figure 14E).

In 2018, the abundance of *C. finmarchicus* was near or below normal in spring and summer, above normal in early fall with unusually large abundances in September and October, and

below normal in late fall (Figure 14A). The abundance of *C. glacialis* remained below normal in spring and summer with the exception of two notably high observations in early June, and increased to near-normal levels in the fall (Figure 14B). The abundance of *C. hyperboreus* remained mostly near or above normal in early spring, increased well above normal in late May and early June, and decreased to near normal levels in the fall (Figure 14C). The abundance of small *Pseudocalanus* spp. copepods was mostly near or below normal in spring and summer and well above normal in early fall (Figure 14D). The abundance of the small *Oithona* spp. copepods decreased from above normal in early spring to below normal in late spring and summer. Abundance increased to above normal for a short period in September and October before declining again to below normal levels in November and December (Figure 14E). The abundance of *T. longicornis* remained low and near normal throughout spring and summer. It then increased well above normal in September and October before returning to near normal levels in late fall, reflecting the trends observed in the other small copepod taxa (Figure 14F).

Copepod phenology

The proportion of adults (CVI) *C. finmarchicus* copepods at S27 typically starts to increase in January and peaks in April at ~45% of all copepodite stages, before declining during spring as newly produced young CI-CIV stages develop throughout the summer. The proportion of CI-CIII remains high (70-80%) from May-July before rapidly declining in late summer as copepodites gradually develop into sub-adults (CV) from August-December (Figure 15A). In 2018, the proportion of adults *C. finmarchicus* peaked in April as usual, although no data were available from January to March (Figure 15B). However, the proportion of adult *C. finmarchicus* in the water column at that time was ~15% higher than the climatology (Figure 15B). The peak timing of CI-CIII copepodites occurred in June, ~1 month later than the climatology. A second peak occurred two months later in August (Figure 15B). The proportion of subadults peaked in October but gave place to a second wave of CIV copepodites in late fall. The proportion of CIV copepodites at the end of 2018 was ~35% higher than usual (Figure 15B).

The proportion of adult *Pseudocalanus* spp. copepods also typically increases during winter to a maximum of ~45% in April, and declines during the spring as CI-CIII copepodites develop (Figure 15C). The proportion of CIV and CV is maximum in the fall when it accounts for ~60% of all *Pseudocalanus* copopodites in the water column (Figure 15C). In 2018, the relative abundance of adult *Pseudocalanus* also peaked in April at a proportion ~15% higher than the climatology. In line with observations for *C. finmarchicus*, the proportion of *Pseudocalanus* CI and CII peaked ~1 month later than usual with a second, less intense peak in August. The proportion of CIV copepodites was ~15% higher than the climatology in late fall (Figure 15D).

Biomass

Dry weight of mesozooplankton are presented for three size classes: total (≤10 mm), small (≤1 mm), and large (1–10 mm) zooplankton. Total zooplankton biomass at S27 is generally lowest in January and increases during the winter to peak in April. Biomass then decreases throughout spring and stabilizes at low levels throughout summer and fall (Figure 16A). The biomass of small zooplankton follows a similar general pattern during winter and spring but slowly increases throughout summer and fall until November when it starts to decline (Figure 16B). The biomass of large zooplankton normally peaks ~2 months later than the small zooplankton. It normally decreases from June to September, and increases again in the fall until November (Figure 16C).

In 2018, total zooplankton biomass was mostly near normal from April-May, above normal from June-October, and below normal in November and December (Figure 16A). The biomass of small zooplankton was below normal in spring, and near or below normal throughout summer

and fall (Figure 16B). Large zooplankton biomass was generally near normal in April-May, despite few unusually high observations in late April. It then remained mostly above the climatology during summer and early fall, and decreased to below normal levels in November (Figure 16C).

ZOOPLANKTON - OCEANOGRAPHIC CROSS-SHELF SECTIONS

Abundance

Copepod abundance shows an overall increasing trend on the Grand Bank (S27, FC, SEGB) since the beginning of the monitoring program, with anomalies transitioning from mostly negative in the early years of the time series to mostly positive toward the end. Near- to above-normal abundances were observed on the Newfoundland Shelf (BB, SI) from 2003–10, but abundance then fluctuated throughout the 2010's (Figure 17A). The increase in copepod abundance in recent years has been more pronounced on the southern Grand Bank (SEGB) than for other sections to the north, with three consecutive record-high anomalies between 2016 and 2018 (Figure 17A). The abundance of non-copepod zooplankton on the Grand Bank also shows an overall increasing trend throughout the 20-year time series, switching from mostly negative to mostly positive anomalies in 2010 (Figure 17B). Abundance of non-copepod on the Newfoundland Shelf varied similarly to that of copepod until the mid-2010's. After that, non-copepod abundance remained above normal until 2018, with several record-highs during that period (Figure 17B). Unlike copepods, the important increase in the abundance of non-copepods organisms in recent years occurred across the entire NL region, reaching levels of 1 to 3 standard deviations above the climatological means (Figure 17B).

The abundance of large calanoid, *C. finmarchicus* was lowest at the beginning of the monitoring program, with strong negative anomalies in most regions of the Grand Bank and the Newfoundland Shelf in 1999 and 2000 (Figure 18A). Abundance remained mostly near or above normal across the NL region from 2001–2013 before declining to below normal levels until 2016. *C. finmarchicus* abundance has increased to near normal in 2017–2018 on most of the Grand Bank, but has remained mostly below normal on the Newfoundland Shelf during the same period (Figure 18A).

The abundance of small calanoid *Pseudocalanus* spp. was also lowest at the beginning of the time series, especially on the Grand Bank where record-low anomalies were observed on all cross-shelf sections (Figure 18B). *Pseudocalanus* spp. abundance remained mostly near or below normal during most of the 2000's on the Grand Bank. Abundance started to increase in 2009 on the Grand Bank and has remained mostly above normal since 2014 across the NL region. *Pseudocalanus* spp. abundance was highest from 2003–2007 on the northern Newfoundland Shelf (SI), and from 2013 until recent years to the south (BB) (Figure 18B).

Trends in the abundance of small cyclopoid *Oithona* spp. aligned with those for *Pseudocalanus* spp. with an overall increase throughout the time series on the Grand Bank, and high abundance from 2002 to 2006 on the Newfoundland Shelf (Figure 18C). Abundance on the southern Newfoundland Shelf (BB) has remained near or above normal since 2003, with the exception of 2012 and 2014 when some of the strongest negative anomalies of the time series were observed. In 2018, *Oithona* spp. abundance was near normal across the region except on the SEGB, where abundance remained high (Figure 18C).

Biomass

Total zooplankton biomass showed similar trends across all oceanographic sections with low biomass in the early years of the time series changing to near or above normal levels from

2002–2011 (Figure 19A). Negative anomalies were observed during the early and mid-2010's but biomass increased again to mostly above normal levels from 2016 onwards (Figure 19A).

The biomass of small (<1 mm) and large (>1 mm) zooplankton showed opposite trends across the time series (Figure 19B, C). The biomass of small zooplankton was mostly below normal at the beginning of the time series, increased to above normal levels from 2002-2006, and declined to below the climatology from 2007–2013. From 2014–2017, the biomass of small zooplankton slightly increased to near normal but declined again in 2018 (Figure 19B).

The biomass of large zooplankton was near normal during the early years of the time series and declined to below normal from the early to mid-2000s (Figure 19C). From 2007–2018, biomass has remained mostly above normal, despite a slight decrease during the early and mid-2010's on some sections (Figure 19C). Annual mean biomass at the coastal high frequency sampling station S27 contrasted with the general regional trend in 2000–2004 and 2012–2015 (Figure 19C). In 2018, the biomass of large zooplankton was above normal across the region with a record high on the northern Newfoundland Shelf (SI) (Figure 19C).

Continuous Plankton Recorder (CPR)

The Continuous Plankton Recorder (CPR) time series provides earlier information on near-surface plankton relative abundance, distribution, and seasonality on the northern Grand Bank and southern Newfoundland prior to the start of the AZMP (1998–1999). The CPR indices differ from the AZMP in that they are derived from information on plankton taxa in the upper 10 m instead of vertical tows integrated through the entire water column. Consequently, CPR indices do not account for the diel vertical migration exhibited by many plankton taxa. Although the CPR time series extends back into the early 1960's, we only present data from 1991 onwards. A significant sampling gap in the CPR occurred during the mid-1970's through to 1990 and again in 2007–2009 which prevented annual relative abundance anomalies to be computed (Figure 20). We generated scorecards of annual anomalies for dominant CPR taxa by combining data along the various commercial vessel transects in the northern Grand Bank and southern Newfoundland regions using 1991–2010 as a reference period to develop the climatology when monthly sampling coverage was sufficient (Figure 21). The commercial vessel tracks in the NL region mostly cover the northern Grand Bank and a smaller portion of the southern Newfoundland Shelf. The southern Newfoundland area encompasses the Green and St. Pierre Banks, portions of Placentia Bay, and portions of the Laurentian Channel (Figure 21).

Annual anomalies generally indicate higher relative abundance of many plankton for the northern Grand Bank compared to southern Newfoundland from 2010–2017 (Figure 22A, B). Higher relative abundances on the northern Grand Bank were also observed in several phytoplankton indices (phytoplankton colour index [PCI], diatoms, and dinoflagellates), and for *C. finmarchicus*, *Oithona spp.* and *Para*/*Pseudocalanus spp.* copepods (Figure 22A, B). Euphausiids, hyperiid amphipods, and acid-sensitive plankton (coccolithophorids, forams, and the pteropod *Limacina* spp.) showed similar trends of above-normal relative abundance on the northern Grand Bank and southern Newfoundland during this time (Figure 22A, B).

The relative abundances of the Arctic copepods *C. glacialis* and *C. hyperboreus* and decapod larvae were generally below normal during 2010–2017 while acid sensitive taxa, copepod nauplii, as well as *Para/Pseudocalanus* spp. and *Oithona spp.* copepods had remarkable positive anomalies of 2 to 5 standard deviations above the climatology (Figure 22A, B). Strong negative anomalies were observed on the northern Grand Bank between the mid-1990's and the mid-2000's for many taxa (Figure 22A). The acid-sensitive taxa also showed generally lower relative abundance from the early time series until the mid-2000's. Several of the copepod and macrozooplankton taxa displayed higher relative abundance during the early 1990's.

The scarcity of the data on the southern Newfoundland Shelf for 2013–2014 and 2016–2017 makes it difficult to contrast the results from that region with the general trend of positive anomalies observed on the northern Grand Bank during the 2010's. There was, however, some suggestion of higher abundance of hyperiid amphipods and acid-sensitive taxa during the 2010's in southern Newfoundland consistent with observations further north (Figure 22B).

Ocean carbon and pH

The solubility of calcium carbonate ($CaCO_3$) in seawater is important to a variety of marine organisms that generate calcified body parts made of aragonite and calcite. The saturation state of $CaCO_3$ (Ω) vary as a function of the acidity (pH) of seawater. Increasing ocean acidity will reduce the saturation horizons (i.e., the depth below which calcification cannot occur) of both forms of carbonate mineral, more so in the case of aragonite compared to calcite. We computed Ω for aragonite and pH at 3 different depth intervals (<50 m, 75–200 m, and >200 m) for the seasonal surveys conducted during 2018 and plotted the average values for each station along the cross-shelf sections. Omega (Ω) values >1 in the spring indicated aragonite saturation at all depth intervals (Figure 23). Ocean pH in the spring was generally >8 in the upper water column (<50 m) but declined below 8 at depths greater than 200 m throughout the survey area (Figure 23). The pH in shallow depths ranged from 7.99 to 8.22 (Total Scale) while Ω ranged from 1.26 to 2.18. At intermediate depths, pH ranged from 7.89 to 8.11 while Ω varied from 1.10 to 1.74. At depths in excess of 200 m, pH ranged from 7.82 to 8.01 and Ω varied from 1.14 to 1.52.

The summer survey extended coverage further north on the Newfoundland Shelf. Ω during summer 2018 was >1 indicating aragonite saturation in the upper and deeper water column in contrast to intermediate depths (75–200 m) where areas of aragonite undersaturation were detected on the northern Grand Bank (Figure 24). In addition, Ω values approaching limiting conditions were observed both in the inshore and offshore zones along the cross-shelf sections on the Newfoundland Shelf and the northern Grand Bank (Figure 24). Ocean pH varied between 7.8 and 8.2 throughout the survey area. Similarly to spring, summer pH generally decreased from near-surface waters to the deep slope waters (Figure 24). In shallow waters, pH values ranged from 7.94 to 8.40 while Ω varied from 1.16 to 2.87. In intermediate waters, pH ranged from 7.84 to 8.11 while Ω varied from 0.86 to 1.78. In deep waters, pH ranged from 7.87 to 8.02, while Ω varied from 1.03 to 1.54.

The fall survey also showed some limited extent of under-saturation in aragonite at deep slope water stations. Omega values <1 were detected at a number of stations on the Grand Bank, Newfoundland Shelf, and Flemish Cap during fall 2018 (Figure 25). Under-saturation of aragonite was typically associated with deep slope waters. In addition, many stations on the Grand Bank at intermediate depths were characterized by conditions approaching the saturation limit (Figure 25). Ocean pH was generally around 8.0 in the upper water-column but decreased with increasing depth. In shallow waters, pH ranged from 7.90 to 8.10 and Ω varied from 1.16 to 2.11. At intermediate depths, pH ranged from 7.86 to 8.22 while Ω varied from 1.02 to 2.27. In deep waters, pH ranged from 7.86 to 8.03, while Ω varied from 0.78 to 1.83.

DISCUSSION

Phytoplankton biomass inferred from optical and chlorophyll indices at the high frequency sampling station (S27) indicate an intense and prolonged spring bloom in 2018. It is unclear what environmental conditions may have favored enhanced production since overall ocean climate conditions in the NL region were characterized as near normal in 2018 (Cyr et al. 2020). A warming of air temperatures was noted in March 2018, which may have helped to stabilize the

upper water-column and allowed surface blooms to initiate earlier than in previous years. In situ observations in March 2018 at S27 were limited but indicated that uptake of nitrate and silicate was underway in the water column during this period. Satellite observations during the latter part of March 2018 also indicated positive anomalies in surface chlorophyll concentration on the northeast Grand Bank and Newfoundland Shelf. A significant freshening was also noted in 2018 along with higher transport of the Labrador Current, which may have also acted to increase stratification of the water column to promote growth of phytoplankton (Tian et al. 2011, Cyr et al. 2020). Higher phytoplankton biomass may also be the result of changes to the timing in the emergence of certain zooplankton taxa. A general decline was observed in integrated indices of the key grazing copepod *C. finmarchicus* since the mid-2010's, which, combined with the delay in copepodite production cycle for that species in 2018 may have reduced grazing pressure and allowed the buildup of phytoplankton biomass. It is somewhat difficult to parse the relative importance of environmental conditions (e.g., stratification) and grazing pressure by zooplankton on phytoplankton production.

In situ chlorophyll concentration in the water column indicated that the spring phytoplankton bloom at S27 was prolonged well into May, when nutrient depletion normally results in a rapid decline in chlorophyll biomass. Both silicate and nitrate inventories in the upper water column were well below the climatology, indicating important uptake of these key limiting macronutrients. Important nutrient uptake to depths in excess of 100 m, which is nearly two times deeper than normal, indicate that a significant portion of the primary production occurred at depth and would not be visible to satellite colour sensors. In line with observations at S27, chlorophyll inventories were near or above normal along the cross-shelf sections on the Grand Banks and the Newfoundland Shelf for a second consecutive year. This marked shift to above normal conditions in phytoplankton biomass at S27 and along the cross-shelf sections in 2018 contrasts with the previous low production period extending back to 2011. Negative anomalies observed throughout the region for shallow and deep nitrate and for shallow silicate in 2018 also support the scenario of increased primary production for that year.

The fall blooms are of weaker intensity compared to the spring blooms. However, positive anomalies of surface chlorophyll concentration were widespread across the Grand Bank and Newfoundland and Labrador shelves in September 2018, indicating an enhanced fall production. The shallow and deep inventories of silicate and nitrate at S27 were also below the climatology in September and October, suggesting significant nutrient uptake by primary producers throughout the water column. However, in situ observations indicated near normal chlorophyll concentrations for the same period, which may be due to a mismatch between sampling and fall bloom peak timing. Moreover, the integrated (0–100 m) chlorophyll inventories are less sensitive to the less intense, surface concentrated fall production and may not have succeeded in identifying the fall bloom.

Broad-scale satellite observations of enhanced spring and fall surface chlorophyll concentrations in 2018 were not entirely consistent with the spring bloom indices at a regional scale. The magnitude and amplitude indices indicated near or below normal conditions in most of the subregions in 2018, despite earlier and longer-lasting blooms compared to previous years. The timing between the spring bloom onset and the emergence of grazing copepods as well as their abundance may influence the intensity of phytoplankton consumption in the water column and may affect the amplitude and magnitude indices.

The overall increase in zooplankton abundance across the NL region since the beginning of the AZMP in 1999 has continued in 2018. The increase in zooplankton abundance is mainly driven by small copepods such as *Pseudocalanus* spp. and *Oithona* spp. The return to near normal abundance levels of numerically dominant *Oithona* spp. copepods across most of the region in 2018 aligns with the general decrease in total copepod abundance compared to the previous

year. However, high abundances of *Pseudocalanus* spp. and *Oithona* spp. on the SEGB largely contributed to the record high anomaly for total copepod abundance on that section in 2018. The sustained high copepod abundance observed on the Grand Bank (S27, FC, SEGB) since 2016 was not as pronounced further north on the Newfoundland Shelf (BB, SI). The increase in the abundance of small copepod taxa that started in the mid 2010's coincided with a decrease in the abundance of large *C. finmarchicus* copepods and marked a shift in the copepod community composition and size structure. Copepods are important in the diet of several species of forage fish including capelin, herring and sand lance. These fish play a key role in the marine food chain by transforming zooplankton production into food available to higher trophic levels (Alder et al. 2008). Past research indicated that the replacement of large *Calanus* copepods (*C. finmarchicus, C. glacialis, C. hyperboreus*) by small and less energy-rich copepods increases visual constraint on foraging, which may negatively impact the efficiency of energy transfer to higher trophic levels even if prey biomass remains constant (van Deurs et al. 2015, Ljungström et al. 2020).

Timing is a key mechanism affecting trophic interactions in temperate environments. Phenological mismatch among trophic levels can have cascading effects on ecosystem community structure (Edwards and Richardson 2004). Timing in the production cycle of *C. finmarchicus* copepods was somewhat delayed at S27 in 2018 relative to the climatology. Although the abundance of adults (CVI) peaked in April as usual, the emergence of CI and CII copepodites occurred in June, one month later than the climatology. A second peak in the abundance of early CI-CIII stages occurred in August. The development of a second generation of *C. finmarchicus* have been observed at S27 (Maillet et al. 2019) and elsewhere in the North Atlantic and Arctic oceans (Gluchowska et al. 2017, Weydmann et al. 2017). Prolonged spring bloom, enhanced fall surface production, and increased temperature at depth from May-July (Cyr et al. 2020) may have favoured the *C. finmarchicus* second generation in 2018 (Head et al. 2013). Emergence of *Pseudocalanus* CI-CII copepodites was also delayed by ~1 month in 2018. Multi-generation production of *Pseudocalanus* have also been observed (Carotenuto et al. 2012). In the present study, *Pseudocalanus* spp. include several species. Therefore, it is uncertain whether the second peak in the abundance of CI-CII copepodites in August 2018 was caused by the development of a second generation due to a lag in the phenology of different *Pseudocalanus* species.

The abundance of non-copepod zooplankton also continued to increase across the region in 2018, reaching either highest or second-highest levels of the time series for each oceanographic section. At S27, increased abundance of non-copepod zooplankton was clearly driven by unusually high abundance of appendicularians during spring and summer 2018. Appendicularians are suspension feeders preying on a wide size range of particles from bacteria to phytoplankton (Diebel 1986). High abundance of appendicularians was also observed in 2016 and 2017 (Maillet et al. 2019) and coincided with an increase in chlorophyll biomass to near or above normal levels after 5 years of low primary production. The increase in the abundance of non-copepod zooplankton started in the early 2010's on the Grand Bank and propagated northward to the Newfoundland Shelf a few years after, suggesting a possible influence of the Gulf Stream in larval transport and advection onto the Grand Bank.

The biomass of mesozooplankton in the North Atlantic is dominated by large, energy-rich calanoid copepods such as *C. finmarchicus*, *C. glacialis*, and *C. hyperboreus* (Planque et al. 1997, Johns et al. 2001, Plourde et al. 2019). These primarily grazing copepods play a key role in the marine food chain by transferring energy from primary producers to higher trophic levels, including planktivorous stages of several ecologically and economically important fish species. *C. finmarchicus* is the most abundant of the large calanoid copepods and the main contributor to zooplankton biomass (Planque et al. 1997). Similar variation patterns between anomaly time

series of *C. finmarchicus* abundance and total zooplankton biomass confirmed the link between the two in Newfoundland and Labrador shelf waters. For example, the increase in *C. finmarchicus* abundance from below to near normal on the Grand Bank in 2017–2018 corresponded to a return of zooplankton biomass to above normal level after several years of mainly negative anomalies. At S27, increased abundance of *C. glacialis* and *C. hyperboreus* in June likely contributed to the high biomass of large zooplankton observed in late spring and early summer and to the above-normal levels for the whole year. Similarly, the decrease in the abundance of the small copeopods *Pseudocalanus* spp. and *Oithona* spp. across the region in 2018 was associated with a decrease in the biomass of small zooplankton. These results reinforced the notion that copepod abundance and community composition are the main drivers controlling the biomass of zooplankton.

Temporal variation in the biomass of small and large zooplankton suggest that an important change occurred in the size structure of the community, characterized by the shift towards more large and less small zooplankton around 2006–2007. These results contrast with the shift from large to small copepods observed in the early 2010's, indicating that changes in zooplankton community composition was not limited to copepods. The general increase in the abundance of shell-bearing pelagic gastropods (mainly *Limacina* spp.) since the mid 2000's, and appendicularians (mainly *Oikopleura* and *Frittilaria* spp.) since the early 2010's (not presented in this report) likely contributed to the overall increase in the biomass of large zooplankton observed since 2007.

The CPR indices of phytoplankton and macrozooplankton taxa on the northern Grand Bank showed levels fluctuating above and below normal during the 2010's while the relative abundance of copepods and acid-sensitive groups increased during the same period. The increase in the relative abundance of copepods was primarily driven by the nauplii, the juvenile of *Calanus*, and smaller *Oithona* spp. and *Para/Pseudocalanus* taxa. Reduction in the relative abundance of the large Arctic calanoid copepod *C. hyperboreus* have been ongoing since the early 2000's. All acid-sensitive taxa, which includes coccolithophorids, foraminiferans, and *Limacina* sp. contributed to the high positive anomalies observed on the northern Grand Bank from 2010 to 2017.

The relative abundance indices for southern Newfoundland also fluctuate above and below normal throughout the 1990's and 2000's. The large increase observed in copepod groups on the northern Grand Bank since the 2010's was not as apparent in southern Newfoundland. It is unclear what drivers are responsible for the increased proportion of acid-sensitive and copepod taxa, but a previous study attributed changes in CPR abundance with general temperature and stratification trends over the North Atlantic (Head and Pepin 2010). The seasonal timing of phytoplankton blooms has important implications for the transfer of energy through trophic levels from primary to secondary and tertiary producers (Cushing 1990, Harrington et al. 1999). Studies also suggest that the timing of plankton cycles in temperate marine systems are sensitive indicators of climate change (Edwards and Richardson 2004). Ocean warming is hypothesized to modify trophic interactions among key planktonic taxa, resulting in the alteration of food web structure, and leading to ecosystem level responses (Beaugrand et al. 2003).

The description of carbonate chemistry along the NL standard cross-shelf sections and at S27 is included in this report series for the first time. The southerly transport of Arctic waters and the local uptake of anthropogenic CO_2 in the deep convective region of the Labrador Sea are the main drivers regulating carbonate chemistry in the northwest Atlantic (Azetsu-Scott et al. 2010, Yashayaev et al. 2014). Long time series of measurements of total alkalinity (TA) and dissolved inorganic carbon (DIC) along with derived pH in the Labrador Sea, indicate DIC has increased by ~0.9 µmol/kg and pH has decreased by ~0.003 units (total scale) per year during 1996–2013 (Yashayaev et al. 2014). Earlier studies of seasonal and spatial variability in ocean carbon

parameters on the Scotian Shelf indicated limited areas of under-saturation of aragonite (Shadwick and Thomas 2014). In addition, localized environmental conditions such as hypoxia in bottom waters of the lower St. Lawrence Estuary has resulted in a significant decline in pH and strong under-saturation of aragonite (Mucci et al. 2011). The increase in ocean acidity related to higher concentrations of anthropogenic CO_2 will continue to impact the saturation state of carbonate minerals. Seasonal measurements of ocean carbon parameters (TA and DIC) are beginning to identify changes in pH conditions and under-saturation of aragonite at intermediate and deeper bottom waters on the Grand Bank, Newfoundland Shelf and Flemish Cap. Changes in the physical marine environment (e.g., warming and increased stratification) together with variable seasonal biological productivity, will continue to influence ocean acidity and carbonate saturation states into the future. The potential impacts of these changes to a variety of marine organisms including primary producers such as coccolithophorids and foraminifera and shell bearing zooplankton is unclear but monitoring of acid-sensitive taxa will remain ongoing within the monitoring program.

SUMMARY

- In general, the chlorophyll biomass measured in situ during seasonal surveys and inferred from broad-scale ocean colour imagery were above the climatology in 2018.
- Silicate and nitrate drawdowns at S27 occurred at depth nearly two-fold deeper than normal in spring 2018, indicating increased primary production throughout most of the water column.
- The shallow (<50 m) and deep (>50 m) macronutrient inventories along the standard ocean sections increased to near normal levels in 2018.
- Chlorophyll inventories from the seasonal oceanographic surveys and at S27 were above normal in 2018.
- The timing and duration of the spring blooms was near-normal over most of the NL subregions in 2018.
- Spring bloom amplitude and magnitude were below normal across most of the NL subregions in 2018.
- The abundance of copepods continued above normal on the Grand Bank in 2018 for a 3rd consecutive year and reached record-high levels on the SEGB section.
- The abundance of non-copepods was well above normal across the NL region with highest or second highest levels for the time series on all sections and at S27.
- The abundance of the large, energy rich Calanus finmarchicus was near to below normal across the NL region except on the northern Newfoundland Shelf (SI), where abundance was slightly above-normal.
- The abundance of small Pseudocalanus spp. and Oithona spp. copepods decreased in 2018 after 2–4 years of unusually high levels.
- The production cycle of C. finmarchicus and Pseudocalanus spp. copepods was delayed at S27 in 2018 with evidence of a second generation for C. finmarchicus.
- The biomass of small zooplankton (<1 mm) was mostly below normal in 2018, while the biomass of large zooplankton (1–10 mm) was above normal across the region with a time-series record high on the northern Newfoundland Shelf (SI).

- Consistent with the zooplankton abundance trends from the AZMP seasonal surveys, the CPR indices of relative abundance indicated recent enhancement of small copepods over the northern Grand Bank and southern NL in recent years.
- Ocean carbon measurements generally indicate that water masses in the NL region are saturated with carbonate ions, but under-saturation of aragonite has been detected at intermediate and deeper bottom waters at certain stations.

ACKNOWLEDGMENTS

We thank the many scientists and technicians at the Northwest Atlantic Fisheries Centre (NAFC) for collecting and providing much of the data contained in this analysis. Carla Caverhill and Cathy Porter at the Bedford Institute of Oceanography provided access to ocean colour data products. We also thank the captains and crews of the CCGS Teleost, CCGS Needler, RV Coriolis II and CCGS Hudson for oceanographic data collection during 2018. We thank Benoit Casault and Stéphane Plourde for reviewing the document.

REFERENCES CITED

Alder, J., Campbell, B., Karpouzi, V., Kaschner, K., and Pauly, D. 2008. Forage Fish: From Ecosystems to Markets. Annu. Rev. Environ. Resour. 33: 153–166.

Azetsu-Scott, K., Clarke, A., Falkner, K., Hamilton, J., Jones, E.P., Lee, C., Petrie, B., Prinsenberg, S., Starr, M., and Yeats, P. 2010. Calcium carbonate saturation states in the waters of the Canadian Arctic Archipelago and the Labrador Sea. J. Geophys. Res. 115, C11021.

Beaugrand, G., Brander, K.M., Lindley, J.A., Souissi, S., and Reid, P.C. 2003. Plankton effect on cod recruitment in the North Sea. Nature. 426: 661–664.

Blais, M., Devine, L., Lehoux, C., Galbraith, P.S., Michaud, S., Plourde, S., and Scarratt, M. 2018. Chemical and Biological Oceanographic Conditions in the Estuary and Gulf of St. Lawrence during 2016. DFO Can. Sci. Advis. Sec. Res. Doc. 2018/037 iv + 57 pp.

Carotenuto, Y., Esposito, F., Pisano, F., Lauritano, C., Perna, M., Miralto, A., and Lanora, A. 2012. Multi-generation cultivation of the copepod *Calanus helgolandicus* in a re-circulating system. J. Exp. Mar. Biol. Ecol. 418–419: 46–58.

Cushing, D.H. 1990. Plankton Production and Year-class Strength in Fish Populations: an Update of the Match/Mismatch Hypothesis. Adv. Mar. Biol. 26: 249–293.

Cyr, F., Colbourne, E., Galbraith, P.S., Gibb, O., Snook, S., Bishop, C., Chen, N., Han, G., and Senciall, D. 2020. Physical Oceanographic Conditions on the Newfoundland and Labrador Shelf during 2018. DFO Can. Sci. Advis. Sec. Res. Doc. 2020/018 iv + 48 p.

DFO. 2019. Oceanographic Conditions in the Atlantic Zone in 2018. DFO Can. Sci. Advis. Sec. Sci. Advis. Rep. 2019/034.

Diebel, D. 1986. Feeding mechanism and house of the appendicularian *Oikopleura vanhoeffeni*. Mar. Biol. 93: 429–436.

Edwards, M., and Richardson, A.J. 2004. Impact of climate change on marine pelagic phenology and trophic mismatch. Nature. 430: 881–884.

Gluchowska, M., Dalpadado, P., Beszcynska-Möller, A., Olszewska, A., Ingvaldsen, R.B., and Kwasniewski, S. 2017. Interannual zooplankton variability in the main pathways of the Atlantic water flow into the Arctic Ocean (Fram Strait and Barents Sea branches). ICES J. Mar. Sci. 74: 1921–1936.

Harrington, R., Woiwod, I., and Sparks, T. 1999. Climate change and trophic interactions. Trends Ecol. Evol. 14(4): 146–150.

Head, E.J.H., and Pepin, P. 2010. Spatial and inter-decadal variability in plankton abundance and composition in the Northwest Atlantic (1958–2006). J. Plank. Res. 32(12): 1633–1648.

Head, E.J.H., Melle, W., Pepin, P., Bagøien, E., and Broms, C. 2013. On the ecology of *Calanus finmarchicus* in the Subarctic North Atlantic: a comparison of population dynamics and environmental conditions in areas of the Labrador Sea-Labrador/Newfoundland Shelf and Norwegian Sea Atlantic and Coastal Waters. Prog. Oceanogr. 114: 46–63.

Johns, D.G., Edwards, M., and Batten, S.D. 2001. Arctic boreal plankton species in the Northwest Atlantic. Can. J. Fish. Aquat. Sci. 58(11): 2121–2124.

Johnson, C., Devred, E., Casault, B., Head, E., Cogswell, A., and Spry, J. 2020. Optical, Chemical, and Biological Oceanographic Conditions on the Scotian Shelf and in the Eastern Gulf of Maine during 2017. DFO Can. Sci. Advis. Sec. Res. Doc. 2020/002. v + 66 p.

Koen-Alonso, M., Pepin, P., Fogarty, M.J., Kenny, A., and Kenchington, E. 2019. The Northwest Atlantic Fisheries Organization Roadmap for the development and implementation of an Ecosystem Approach to Fisheries: structure, state of development, and challenges. Mar. Policy. 100: 342–352.

Ljungström, G., Claireaux, M., Fiksen, Ø., and Jørgensen, C. 2020. Body size adaptations under climate change: zooplankton community more important than temperature or food abundance in model of a zooplanktivorous fish. Mar. Ecol. Prog. Ser. 636: 1–18.

Maillet, G., Bélanger, D., Doyle, G., Robar, A., Fraser, S., Higdon, J., Ramsay, D., and Pepin, P. 2019. Optical, Chemical, and Biological oceanographic conditions on the Newfoundland and Labrador Shelf during 2016–2017. DFO Can. Sci. Advis. Sec. Res. Doc. 2019/055. viii + 35 p.

Mitchell, M.R., Harrison, G., Pauley, K., Gagné, A., Maillet, G., and Strain, P. 2002. Atlantic Zonal Monitoring Program sampling protocol. Can. Tech. Rep. Hydrogr. Ocean Sci. 223: iv + 23 pp.

Mucci, A., Starr, M., Gilbert, D., and Sundby, B. 2011. Acidification of Lower St. Lawrence Estuary Bottom Waters. Atmos-Ocean 49(3): 206–218.

O'Reilly, J.E., Maritorena, S., Mitchell, B.G., Siegel, D.A., Carder, K.L., Garver, S.A., Kahru, M., and McClain, C. 1998. Ocean color chlorophyll algorithms for SeaWiFS. J. Geophys. Res.103(C11): 24937–24953.

Planque, B., Hays, G.C., Ibanez, F., and Gamble, J.C. 1997. Large scale spatial variations in the seasonal abundance of *Calanus finmarchicus*. Deep Sea Res. Part I: Ocean. Res. Pap. 44(2): 315–326.

Platt, T., Sathyendranath, S., Caverhill, C.M., and Lewis, M.R. 1988. Ocean primary production and available light: further algorithms for remote sensing. Deep Sea Res. Part I: Ocean. Res. Pap. 35(6): 855–879.

Plourde, S., Lehoux, C., Johnson, C.L., Perrin, G., and Lesage, V. 2019. North Atlantic right whale (*Eubalena glacialis*) and its food: (I) a spatial climatology of *Calanus* biomass and potential foraging habitats in Canadian waters. J. Plankton Res. 41(5): 667–685.

Shadwick, E.H., and Thomas, H. 2014. Seasonal and spatial variability in the CO_2 system on the Scotian Shelf (Northwest Atlantic). Mar. Chem. 160: 42–55.

Therriault, J.-C., Petrie, B., Pepin, P., Gagnon, J., Gregory, D., Helbig, J., Herman, A., Lefaivre, D., Mitchell, M., Pelchat, B., Runge, J., and Sameoto, D. 1998. Proposal for a Northwest Atlantic Zonal Monitoring Program. Can. Tech. Rep. Hydrogr. Ocean Sci. 194: vii+57 p.

Tian, T., Su, J., Flöser, G., Wiltshire, K., and Wirtz, K. 2011. Factors controlling the onset of spring blooms in the German Bight 2002–2005: Light, wind and stratification. Cont. Shelf Res. 31(10): 1140–1148.

Van Deurs, M., Jørgensen, C., and Fiksen, Ø. 2015. Effects of copepod size on fish growth: a model based on data for North Sea sandeel. Mar. Ecol. Prog. Ser. 520: 235–243.

Weydmann, A., Walczowski, W., Carstensen, J., and Kwaśniewski, S. 2017. Warming of Subarctic waters accelerates development of a key marine zooplankton *Calanus finmarchicus*. Global Change Biol. 24(1): 172–183.

Yashayaev, Head, E.J.H., Azetsu-Scott, K., Wang, Z., Li, W.K.W., Greenan, B.J.W., Anning, J., and Punshon, S. 2014. Oceanographic and Environmental Conditions in the Labrador Sea during 2012. DFO Can. Sci. Advis. Sec. Res. Doc. 2014/046 v + 24 p.

Zhai, L., Platt, T., Tang, C., Sathyendranath, S., and Walls, R.H. 2011. Phytoplankton phenology on the Scotian Shelf. ICES J. Mar. Sci. 68(4): 781–791.

TABLES

Table 1. Atlantic Zone Monitoring Program sampling surveys in Newfoundland and Labrador Region in 2018. Hydro stations are the total sum of CTD profiles conducted during respective missions including both partial stations (CTD/XBT only) and complete occupations including CTD profile, water sampling and net tows.

Group	Location	Mission ID	Dates	# Hydro Stations	# Net / Bottle Stations
Spring Ecosystem Trawl Surveys	NE Newfoundland Shelf and Grand Bank	TEL2018–159–172	May 10–Jun 21, 2018	498	6 / 5
Fall Ecosystem Trawl Surveys	Grand Bank, NE Newfoundland and Labrador Shelf	NED2018–464–472, TEL2018–162–167	Aug 21–Dec 20, 2018	643	17 / 9
Spring AZMP Survey	Grand Bank and NE Newfoundland Shelf	TEL2018–185	Apr 6–24, 2018	112	55 / 56
Summer AZMP Survey	Grand Bank, NE Newfoundland and Labrador Shelf	COR2018–011	Jul 15–Aug 2, 2018	169	83
Fall AZMP Survey	Grand Bank and NE Newfoundland Shelf	HUD118	Nov 11–Dec 2, 2018	134	75 / 73
Station 27 Occupations	Avalon Channel	Ships of Opportunity	Mar 8–Dec 18, 2018	36	18 / 8

FIGURES

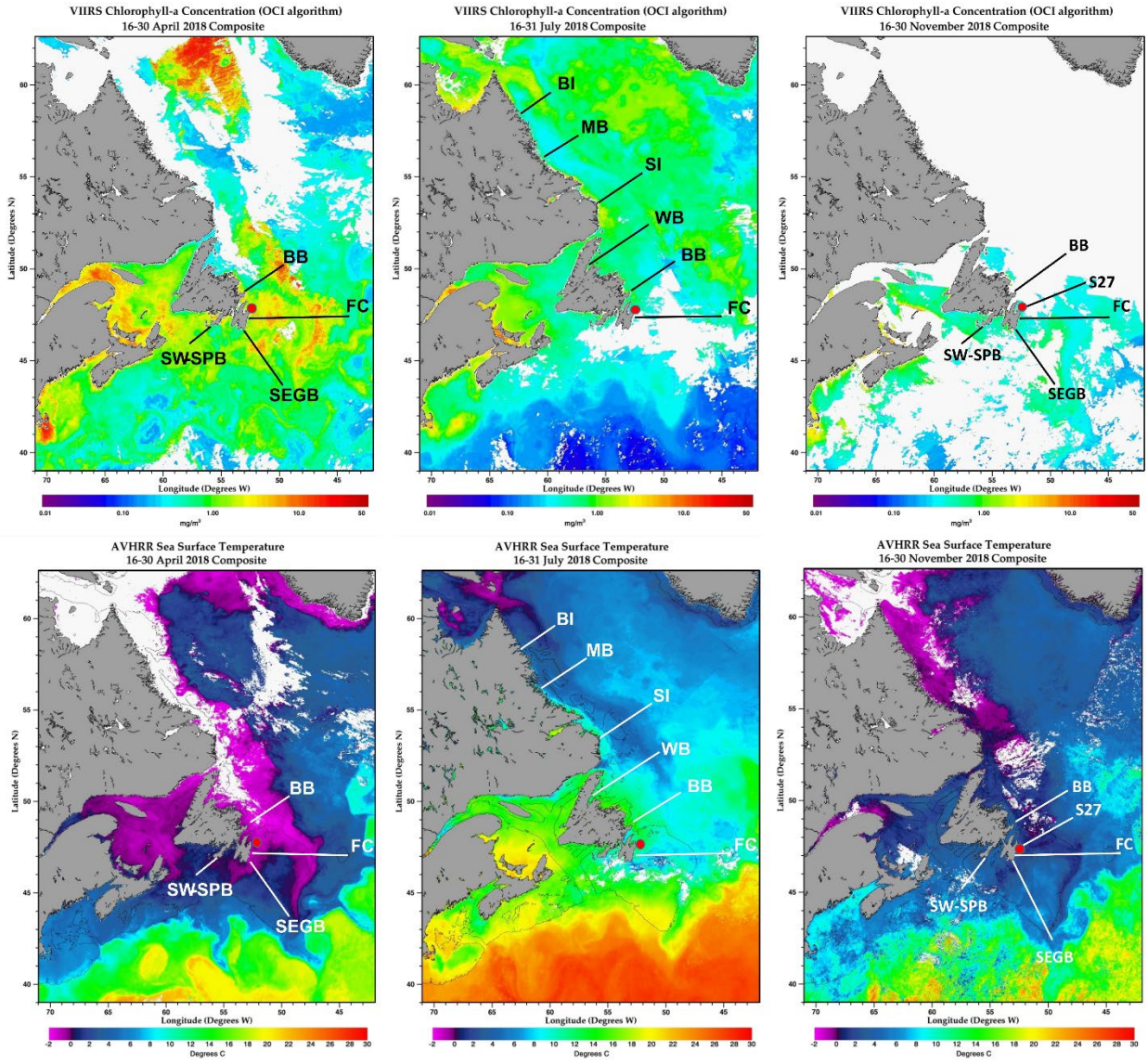

Figure 1. Location of cross-shelf sections (BI-Beachy Island, MB=Makkovik Bank, SI=Seal Island, WB=White Bay, BB=Bonavista Bay, FC=Flemish Cap, SEGB=Southeast Grand Bank, SW-SPB=Southwest St. Pierre Bank) and high-frequency sampling station S27 (red circle) occupied during the spring (left panels), summer (middle panels), and fall (right panels) 2018 AZMP surveys along with mean surface chlorophyll concentration (top panels) and sea surface temperature (bottom panels) at the time of sampling.

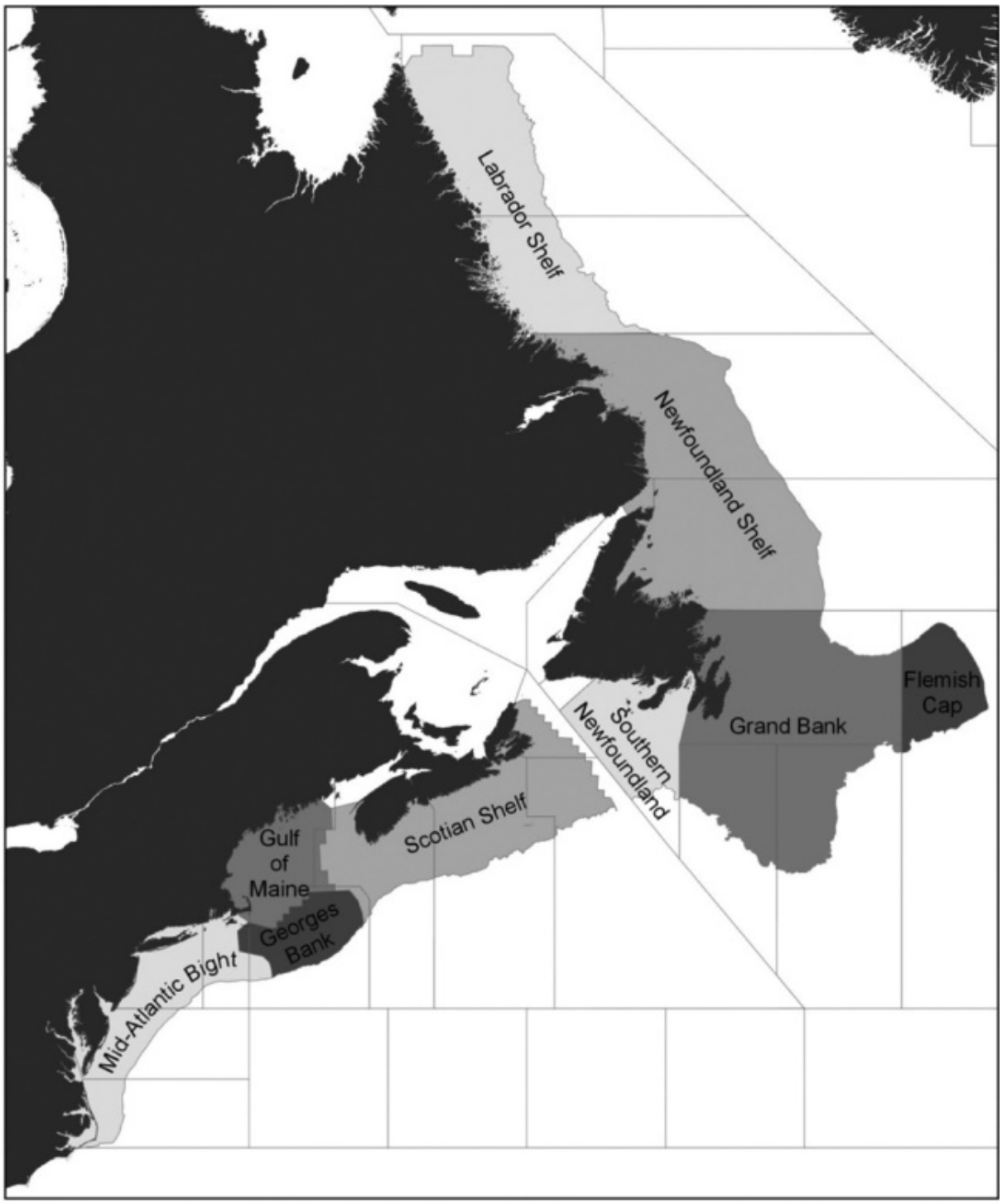

Figure 2. NAFO's Ecosystem Production Units (EPUs) used in the present report to refer to the different subregions of the Newfoundland and Labrador continental shelf which include the Labrador Shelf, the Newfoundland Shelf, the Flemish Cap, the Grand Bank, and the Southern Newfoundland subregions. Figure from Koen-Alonso et al. 2019.

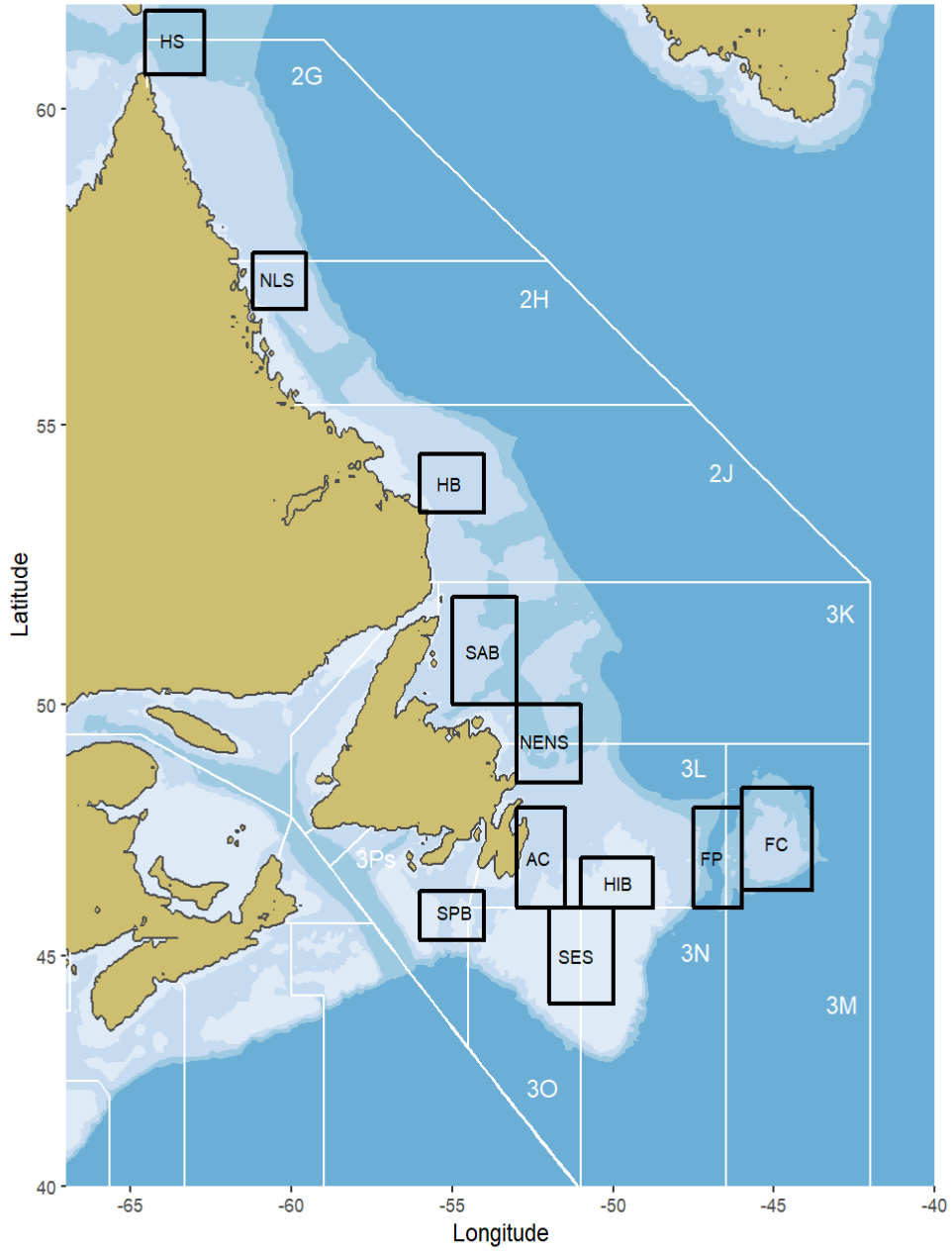

Figure 3. Location of subregions from which phytoplankton spring bloom metrics (initiation, duration, amplitude and magnitude) are derived from ocean colour satellite observations. HS=Hudson Strait, NLS=Northern Labrador Shelf, HB=Hamilton Bank, SAB=St. Anthony Basin, NENS=Northeast Newfoundland Shelf, AC=Avalon Channel, HIB=Hibernia, FP=Flemish Pass, FC=Flemish Cap, SES-Southeast Shoal, SPB=St. Pierre Bank.

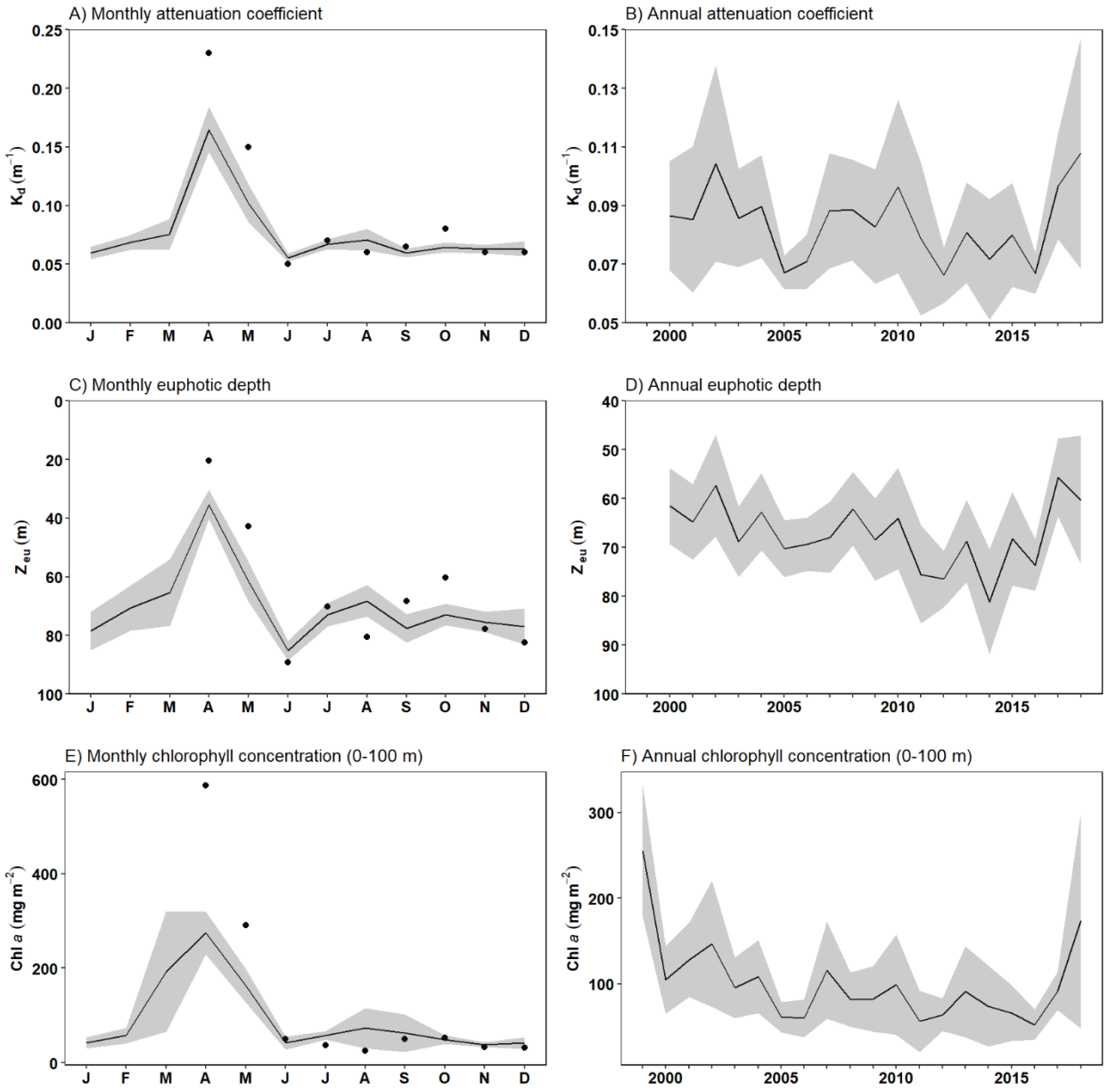

Figure 4. Monthly (left panels) and annual (right panels) mean vertical light attenuation coefficient (A, B), euphotic depth (C, D), and integrated chlorophyll a concentration (E, F) at the high frequency sampling station S27. Black line and grey ribbon indicate the mean (±95% CI) for the 2000–2015 climatology. Black dots indicate monthly mean for the year 2018. Letters on the abscissas are month of the year.

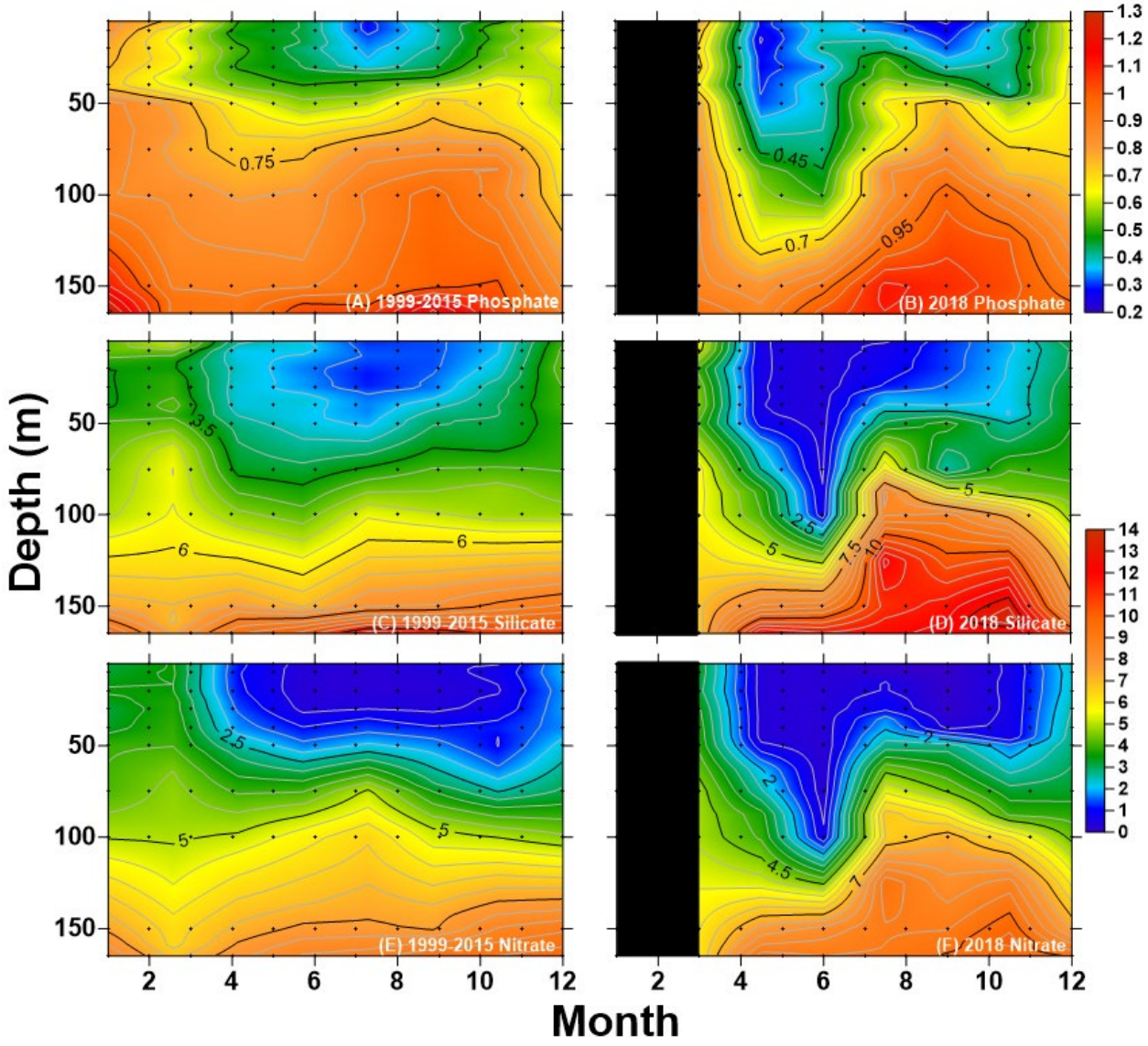

Figure 5. Comparison of vertical structure of phosphate (A, B), silicate (C, D) and nitrate (E, F) in mmol m^{-3} between the 1999–2015 climatology (left panels) and 2018 (right panels) at the high frequency sampling coastal station S27. Gridding method to generate contour plots using triangulation with linear interpolation. Black dots indicate interpolated grid and standard sampling depths. Missing monthly observations in 2018 are shown in solid black.

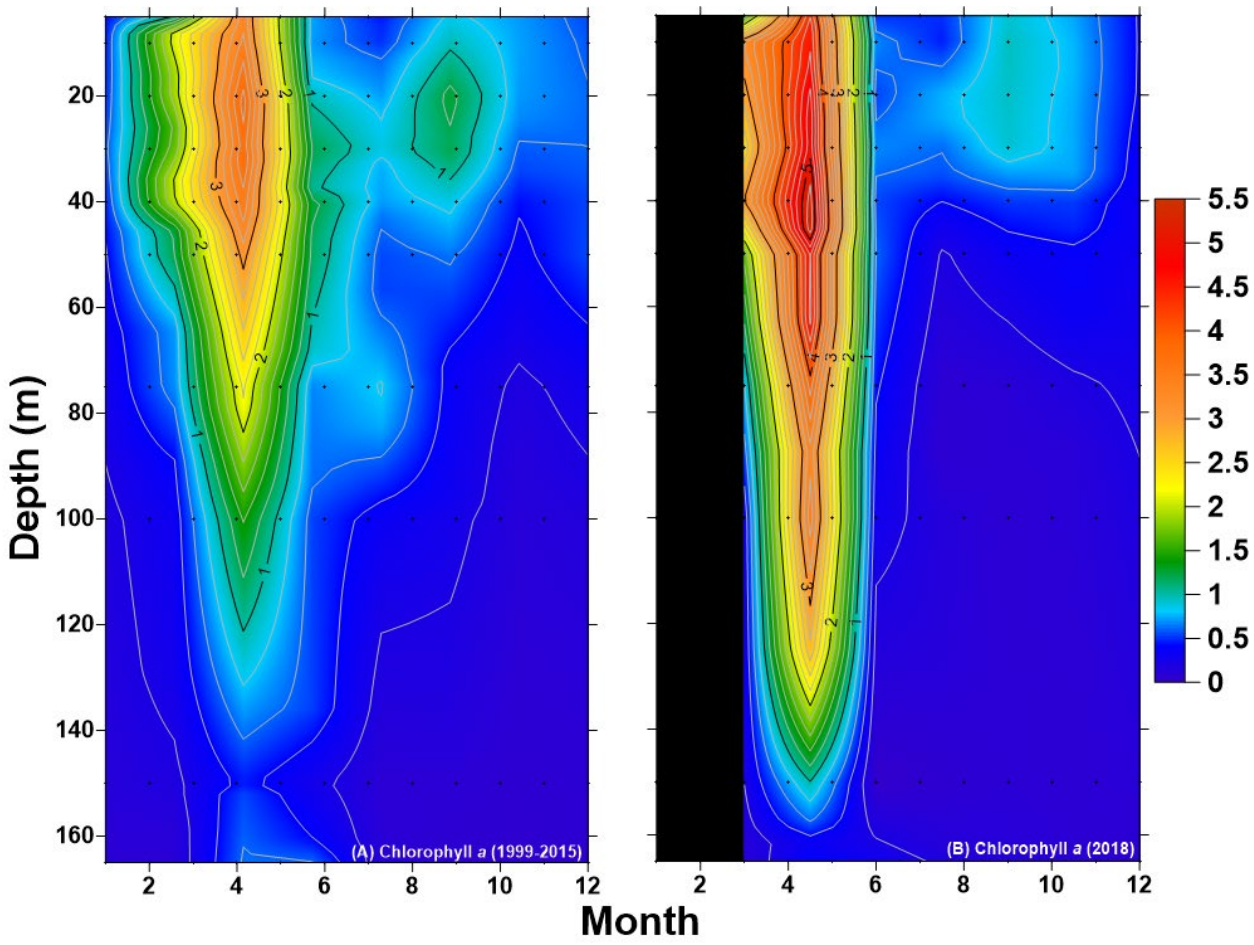

Figure 6. Comparison of the vertical structure of chlorophyll a concentration in mg m^{-3} between (A) the 1999–2015 climatology, and (B) the year 2018 at the high frequency sampling station S27. Gridding method to generate contour plots using triangulation with linear interpolation. Black dots indicate interpolated grid and standard sampling depths. Missing monthly observations in 2018 are shown in solid black.

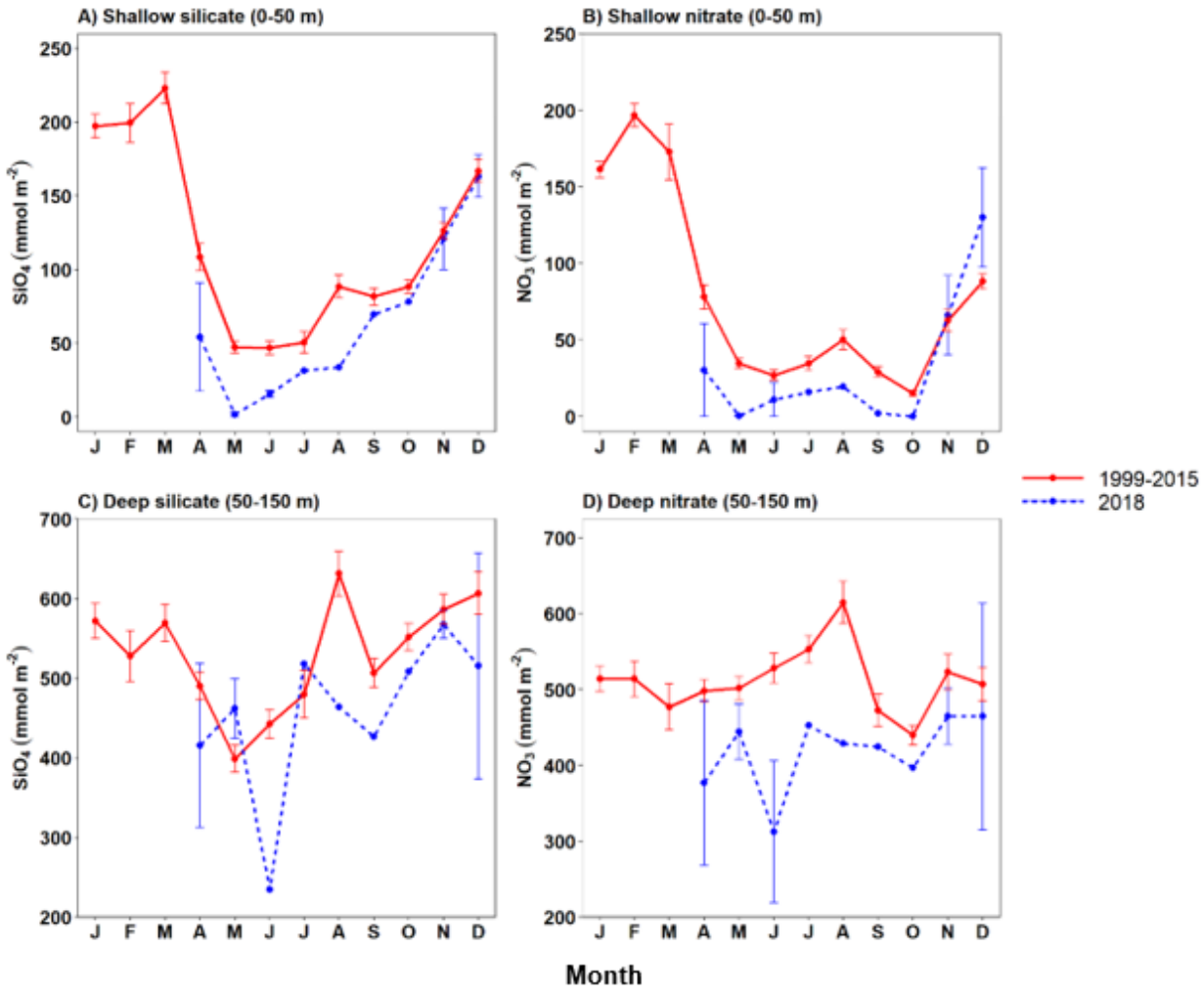

Figure 7. Comparison of annual variability in shallow (top panels) and deep (bottom panels) silicate (left panels) and nitrate (right panels) inventories between the 1999–2015 climatology and 2018 at the high frequency sampling station S27. The vertical lines are the standard error of the monthly means. No observations were available in January through March 2018.

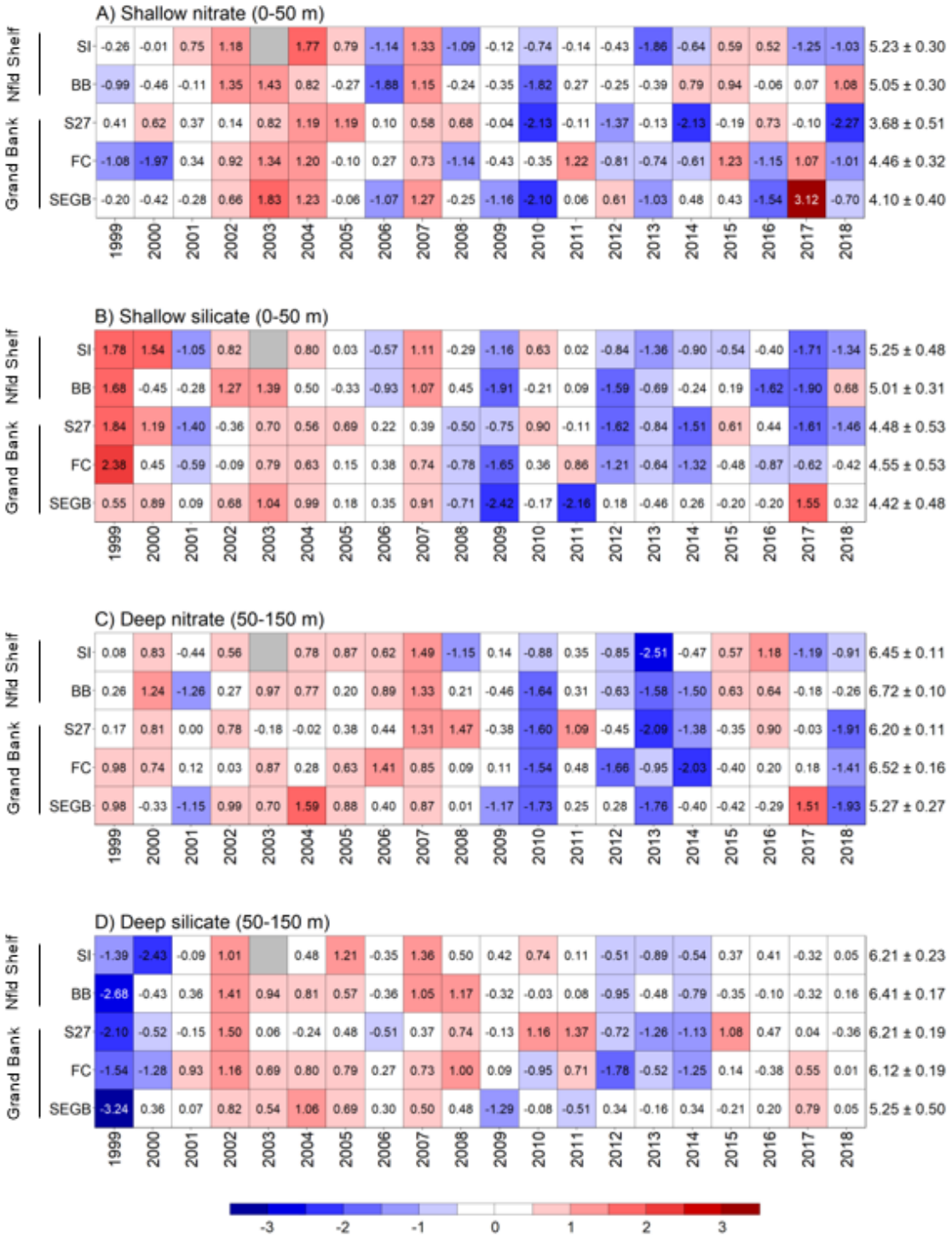

Figure 8. Annual anomaly scorecard for shallow (A, C) and deep (B, D) nitrate and silicate inventories. Numbers in each cell are anomalies from the mean for the 1999–2015 climatology in standard deviation units (mean [ln 1+ concentration in mmol m^{-2}] and SD listed at right). Grey cells indicate missing data. Red (blue) cells indicate higher (lower) than normal concentration. White cells indicate near normal concentration. Sections are listed from north (top) to south (bottom). SI: Seal Island; BB: Bonavista Bay; S27: Station 27; FC: Flemish Cap; SEGB: Southeast Grand Bank. See Figure 1 for section geographical location.

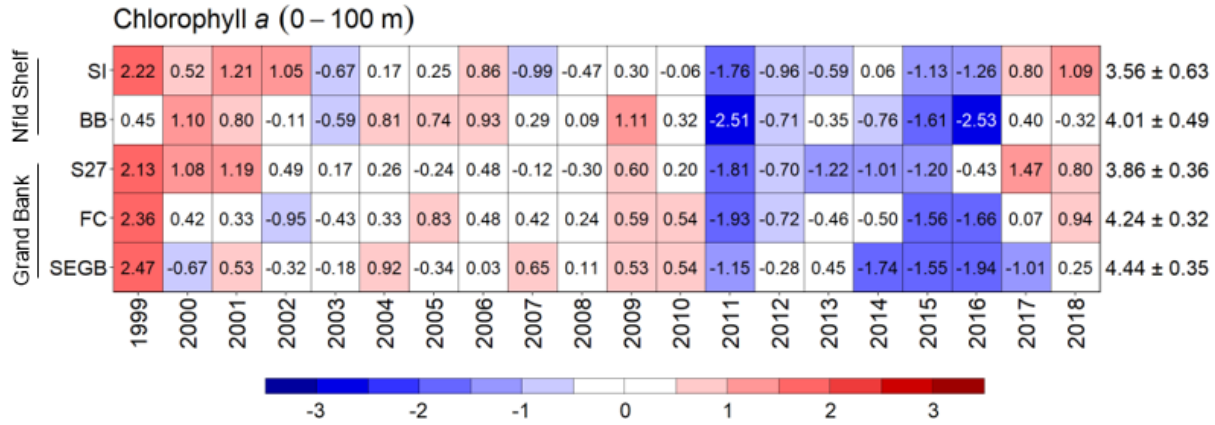

Figure 9. Annual anomaly scorecard for integrated chlorophyll a inventories. Numbers in each cell are anomalies from the mean for the1999–2015 climatology, in standard deviation units (mean [ln 1+ concentration in mg m^{-2}] and SD listed at right). Red (blue) cells indicate higher (lower) than normal concentration. White cells indicate near normal concentration. Sections are listed from north (top) to south (bottom). SI: Seal Island; BB: Bonavista Bay; S27: Station 27; FC: Flemish Cap; SEGB: Southeast Grand Bank. See Figure 1 for section geographical location.

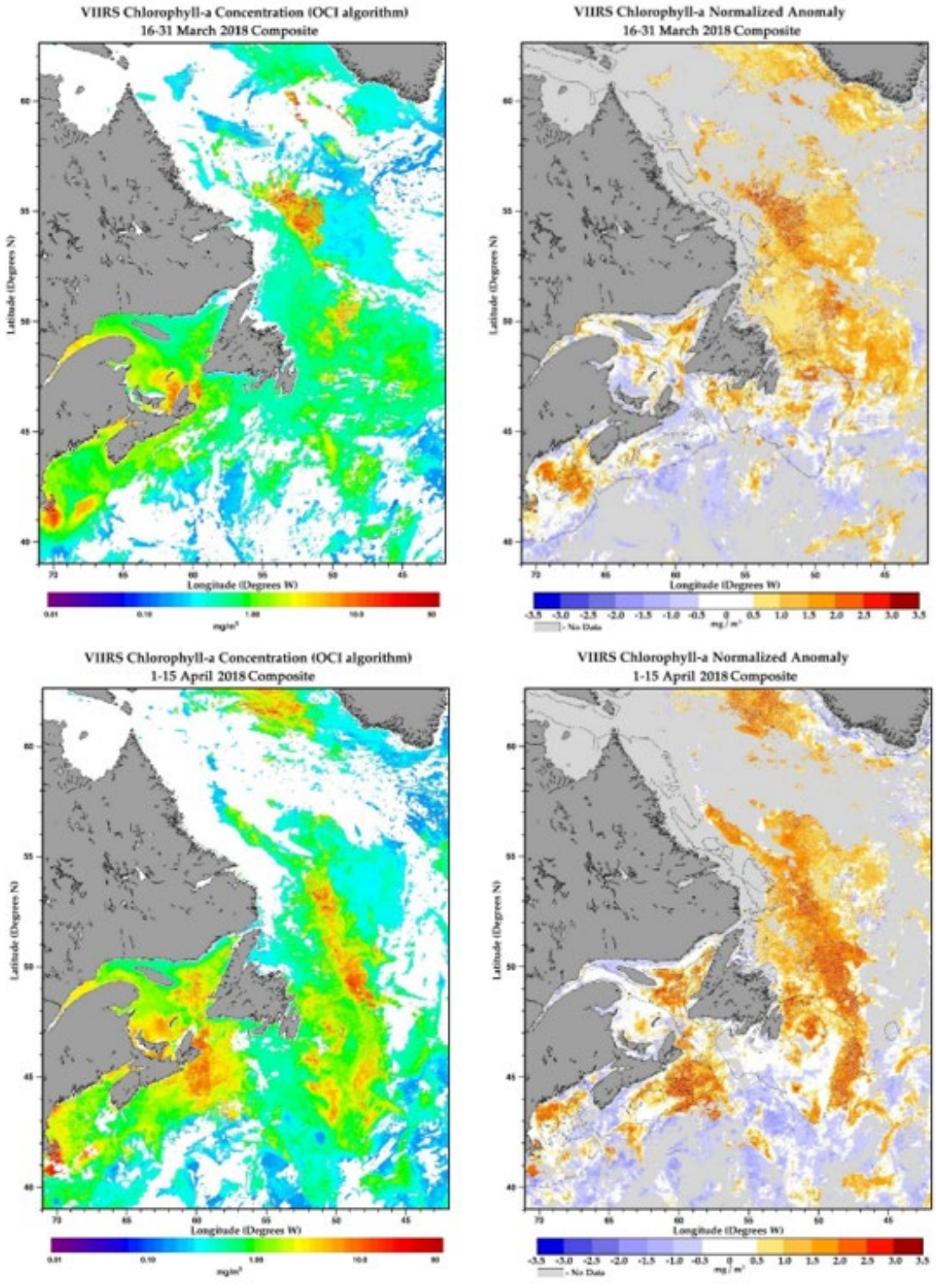

Figure 10. Semi-monthly surface chlorophyll a concentrations (left panels) and standardized anomalies based on a 1998–2015 climatology (right panels) from VIIRS ocean colour imagery in the North Atlantic during spring 2018. Panels are semi-monthly composite imagery from late March (top panels) to the end of May (bottom panels). White (grey) areas on the left (right) panels indicate no data available due to ice-cloud-covered periods.

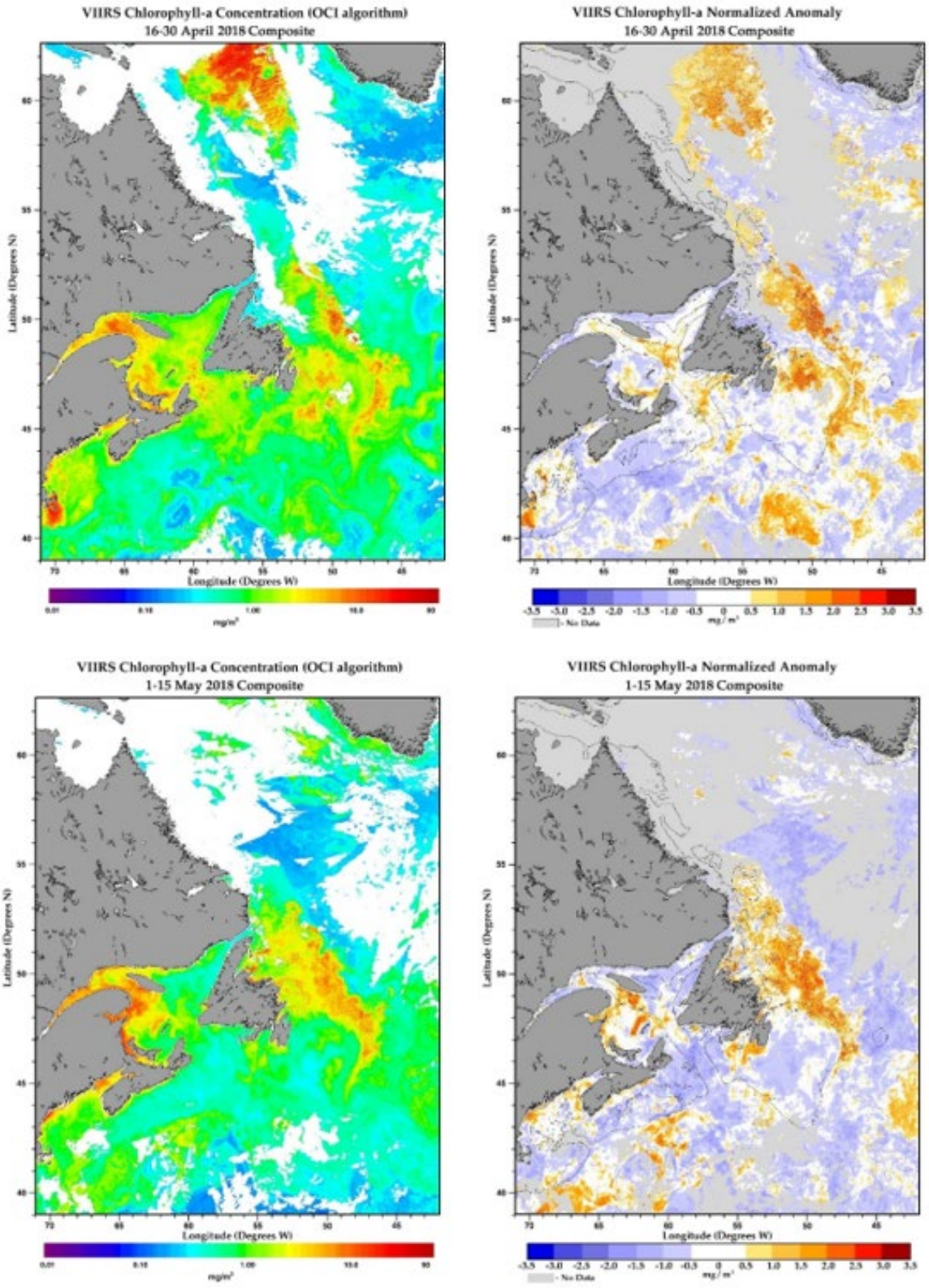

Figure 10 continued.

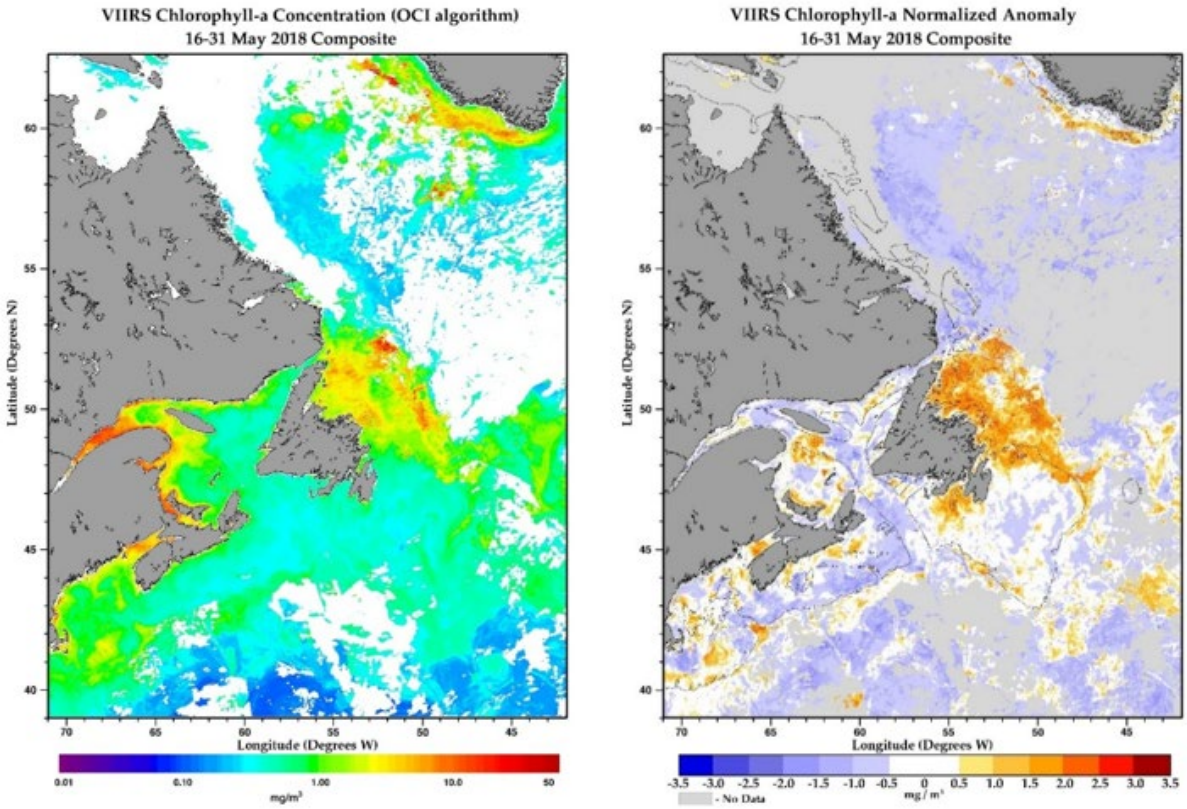

Figure 10 continued.

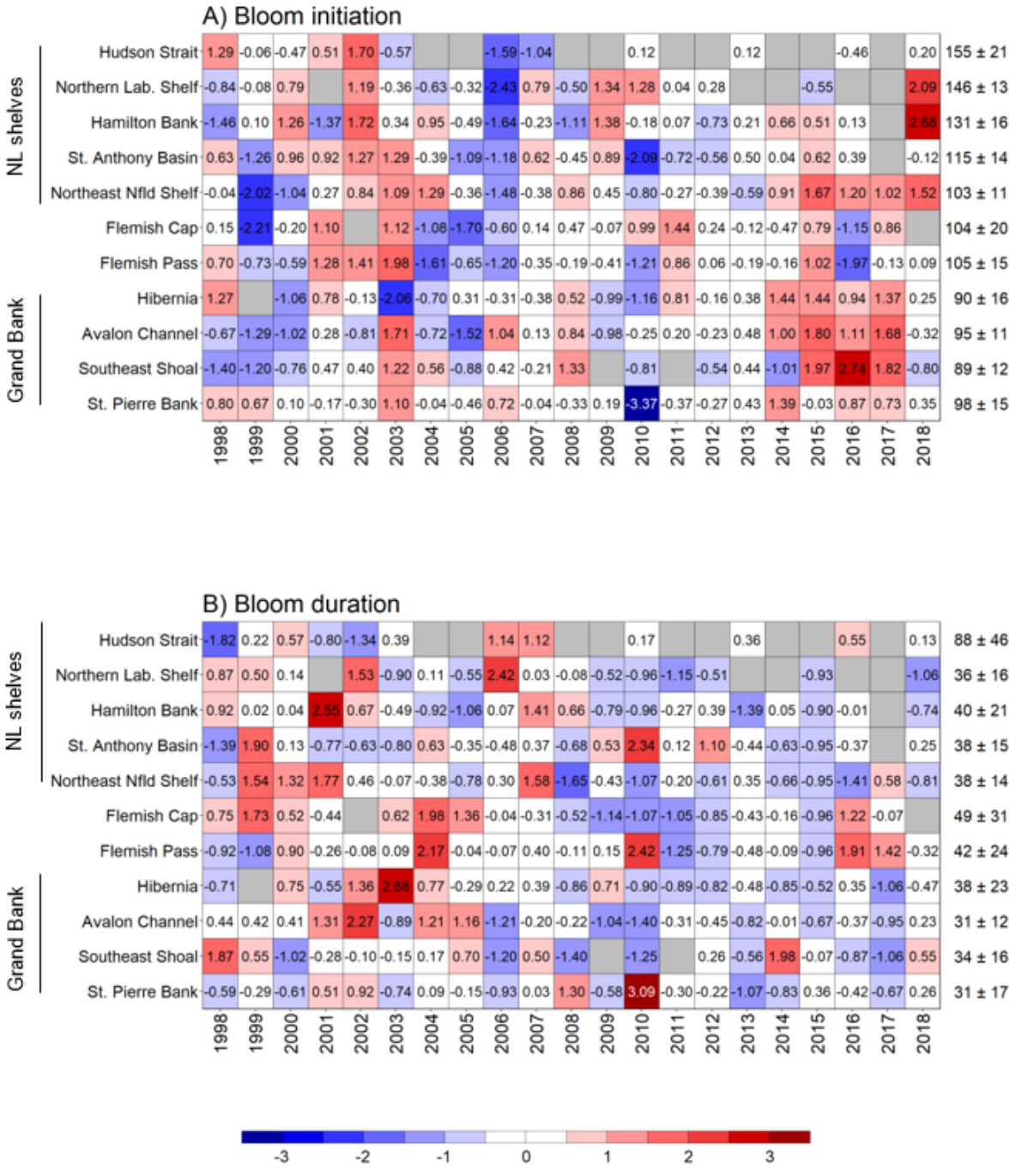

Figure 11. Annual anomaly scorecards for spring bloom metrics. Numbers in each cell are anomalies from the mean for the 1998–2015 climatology in standard deviation units (mean and SD listed at right). Grey cells indicate missing data. Red (blue) cells indicate later (earlier) initiation, longer (shorter) duration or higher (lower) amplitude or magnitude than normal. White cells indicate near normal conditions. Climatological means are in Julian day for the bloom initiation, in days for the duration, and in mg m^{-3} for the amplitude, and in mg m^{-2} d^{-1} for the magnitude of the bloom. Subregions are listed from north (top) to south (bottom). See Figure 3 for subregions geographical location.

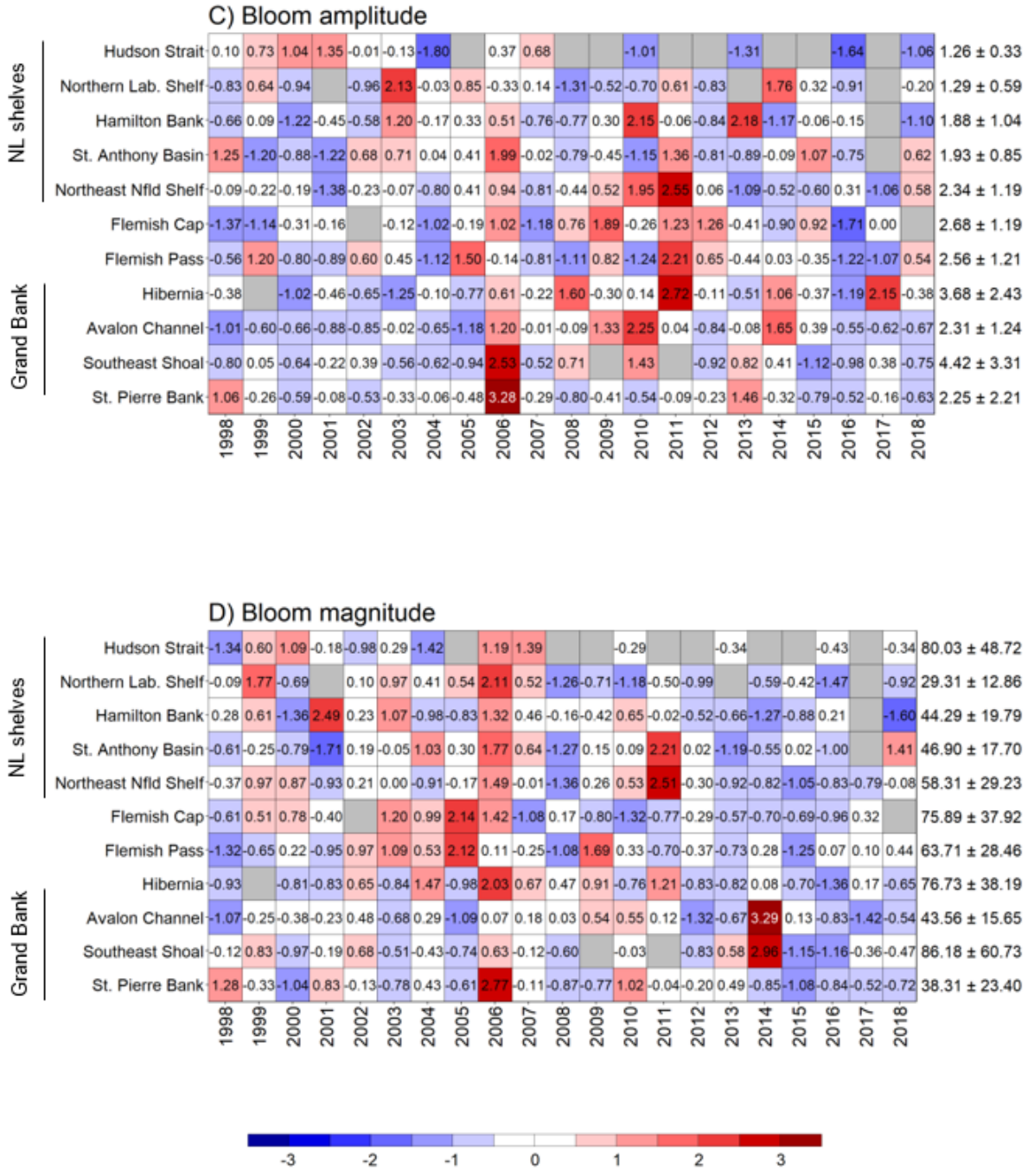

Figure 11 continued.

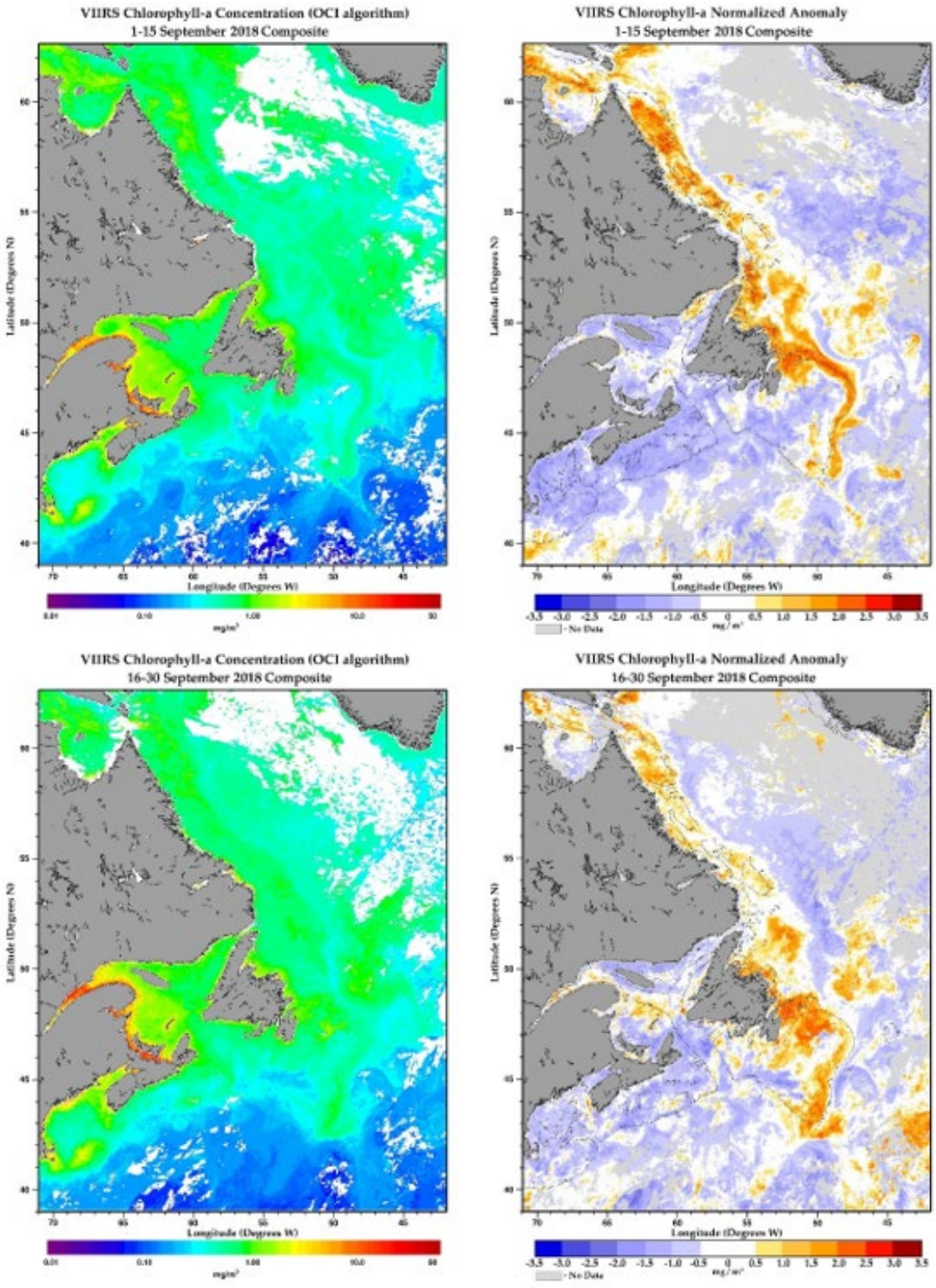

Figure 12. Semi-monthly surface chlorophyll a concentrations (left panels) and standardized anomalies based on a 1998–2015 climatology (right panels), from VIIRS ocean colour imagery in the North Atlantic during fall 2018. Panels are semi-monthly composite imagery from the first (top) and second (bottom) half of September. White (grey) areas on the left (right) panels indicate no data available due to ice-cloud-covered periods.

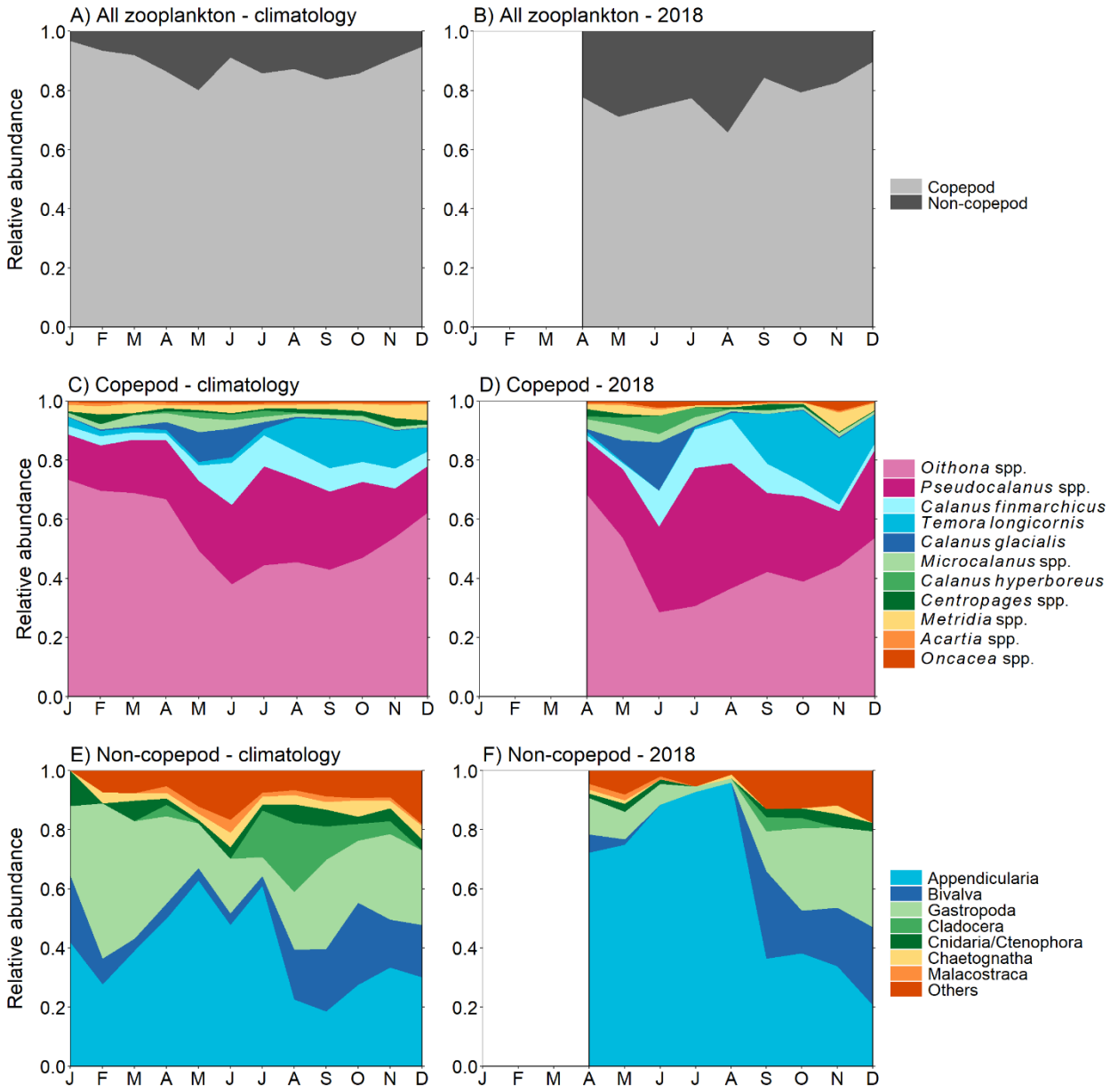

Figure 13. Relative abundance of copepod and non-copepod mesozooplankton (A, B), main copepod taxa (C, D), and main non-copepod taxa (E, F) for the 1999–2015 climatology (left panels) and 2018 (right panels) at the high frequency sampling coastal station S27. Relative abundance were calculated using monthly mean concentrations of the different taxa. Letters on the abscissas are months of the year.

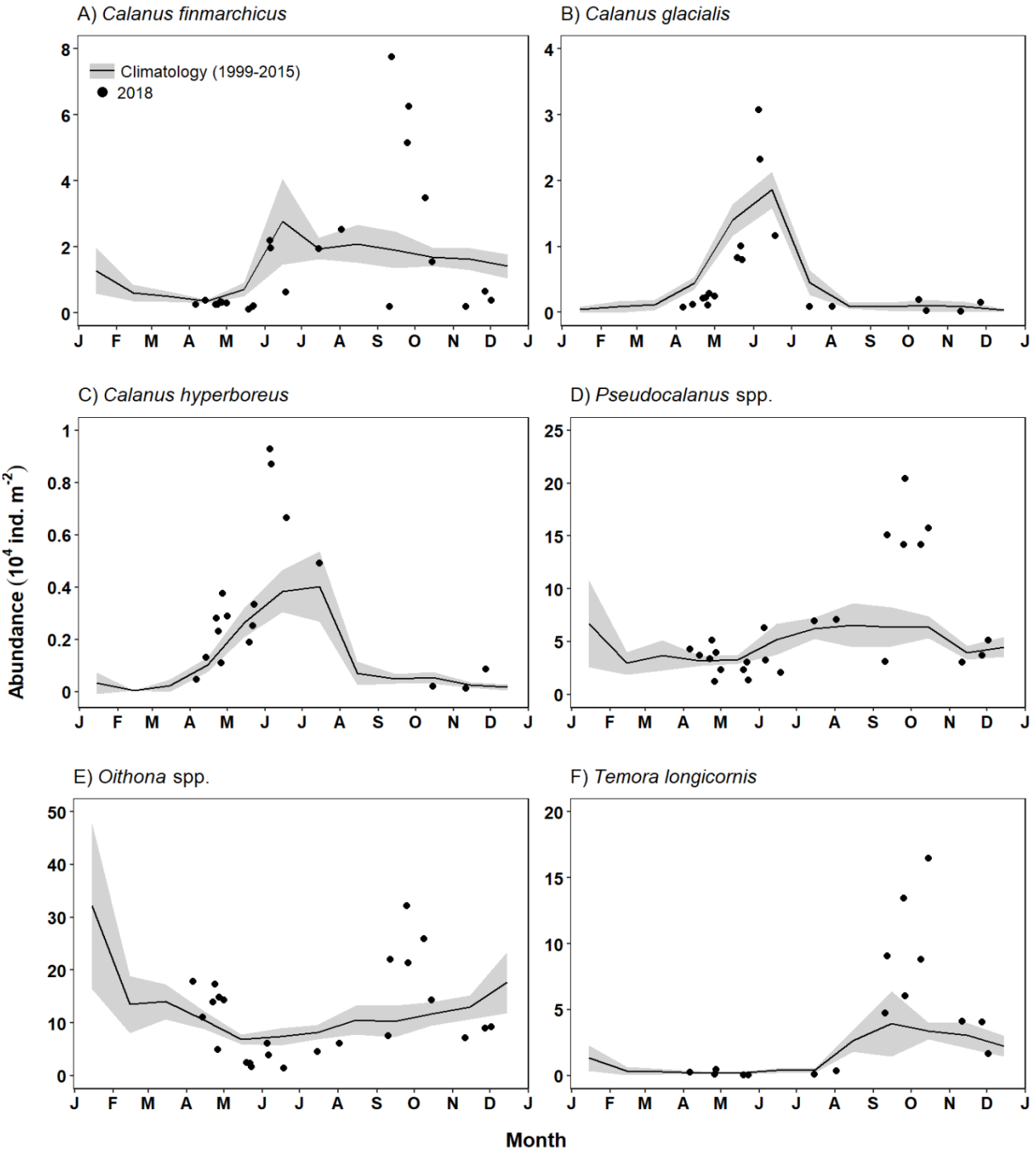

Figure 14. Seasonal variation in the abundance of ecologically important copepod taxa at the high frequency sampling station S27. Black line and grey ribbon indicate monthly mean (±95% CI) abundance for the 1999–2015 climatology. Black dots indicate abundances on each station occupation during 2018. Letters on the abscissas are months of the year.

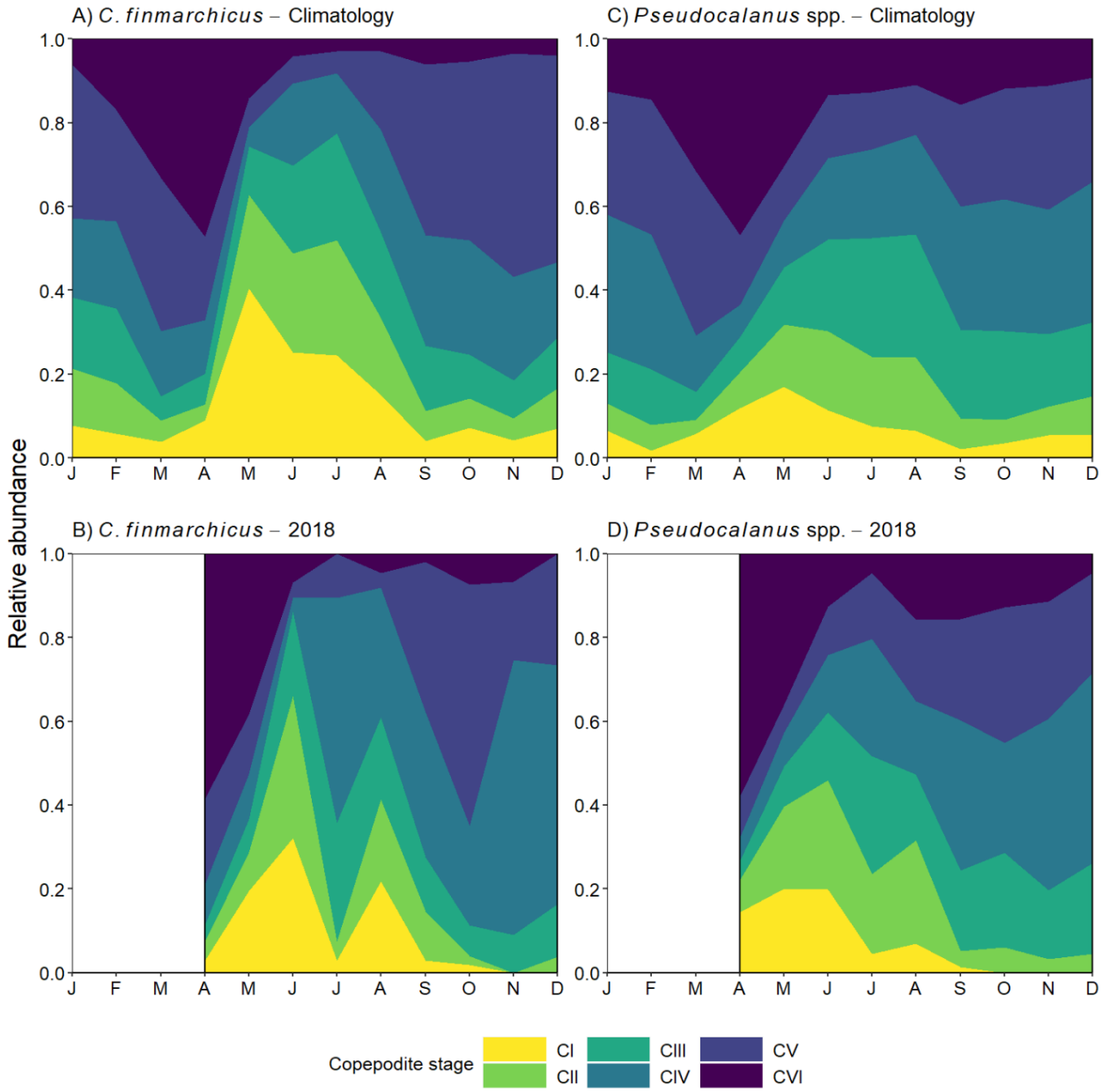

Figure 15. Seasonal variation in the relative abundance of Calanus finmarchicus (A, B) and Pseudocalanus spp. (C, D) copepodite stages for the 1999–2015 climatology (left panels) and 2018 (right panels) at the high frequency sampling coastal station S27. Relative abundance were calculated using monthly mean concentrations of the different copepodite stages. Letters on the abscissas are months of the year.

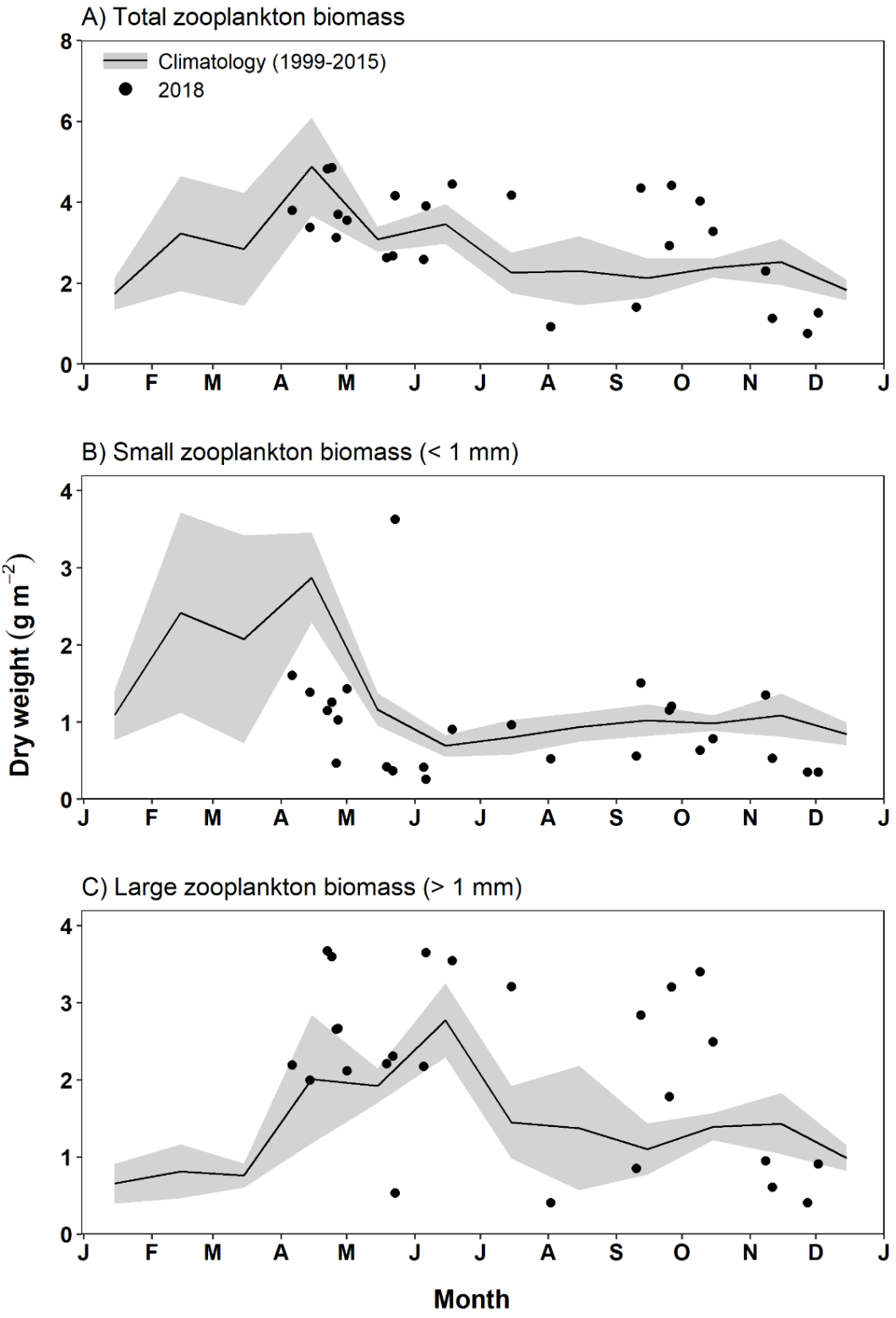

Figure 16. Seasonal variation in the total (<10 mm) zooplankton biomass (A), and for the small (≤1 mm) (B) and large (1–10 mm) (C) zooplankton size fraction at the high frequency sampling coastal station S27. Black line and grey ribbon indicate monthly mean (±95% CI) abundance for the 1999–2015 reference period. Black dots indicate biomass on each station occupation during 2018.

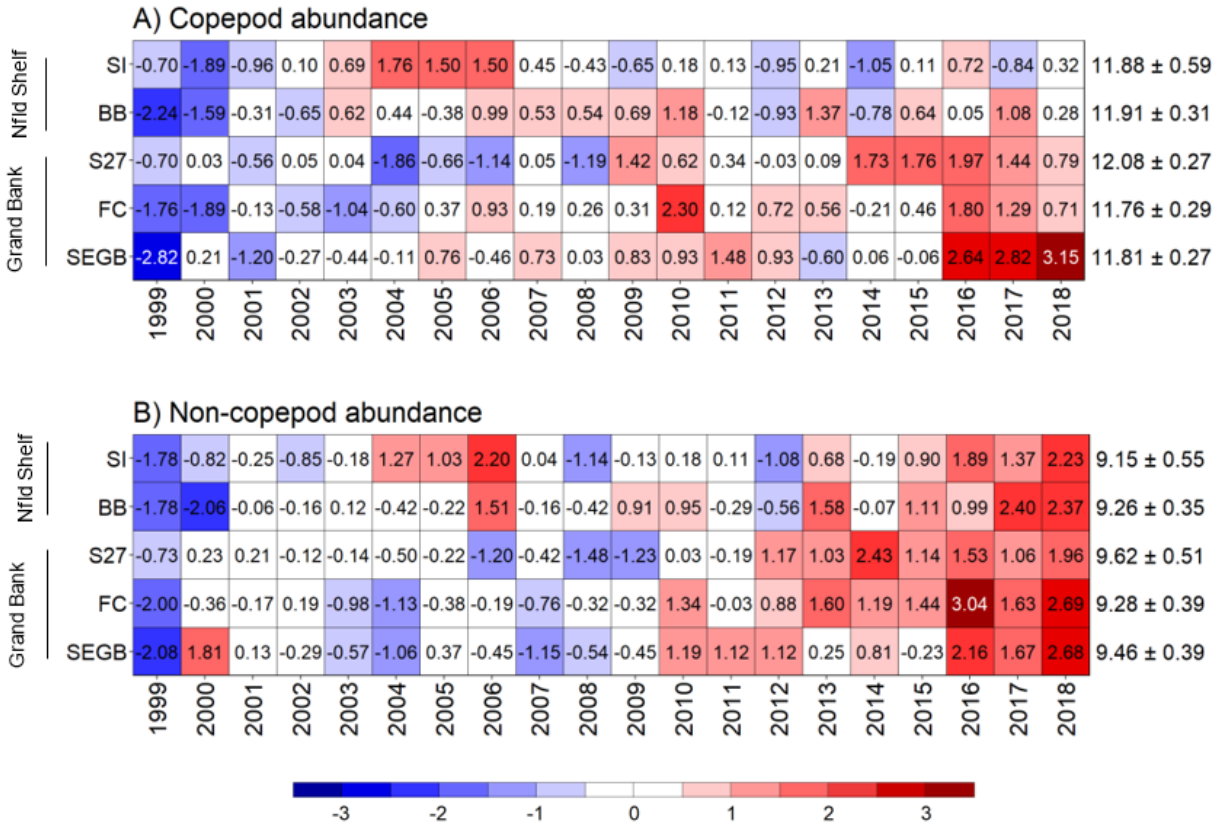

Figure 17. Annual anomaly scorecards for (A) copepod and (B) non-copepod abundance. Numbers in each cell are anomalies from the mean for the 1999–2015 climatology in standard deviation units (means [ln 1 + concentration in ind. m^{-2}] and SD listed at right). Red (blue) cells indicate higher (lower) than normal abundance. White cells indicate near normal abundance. Sections are listed from north (top) to south (bottom). SI: Seal Island; BB: Bonavista Bay; S27: Station 27; FC: Flemish Cap; SEGB: Southeast Grand Bank. See Figure 1 for section geographical location.

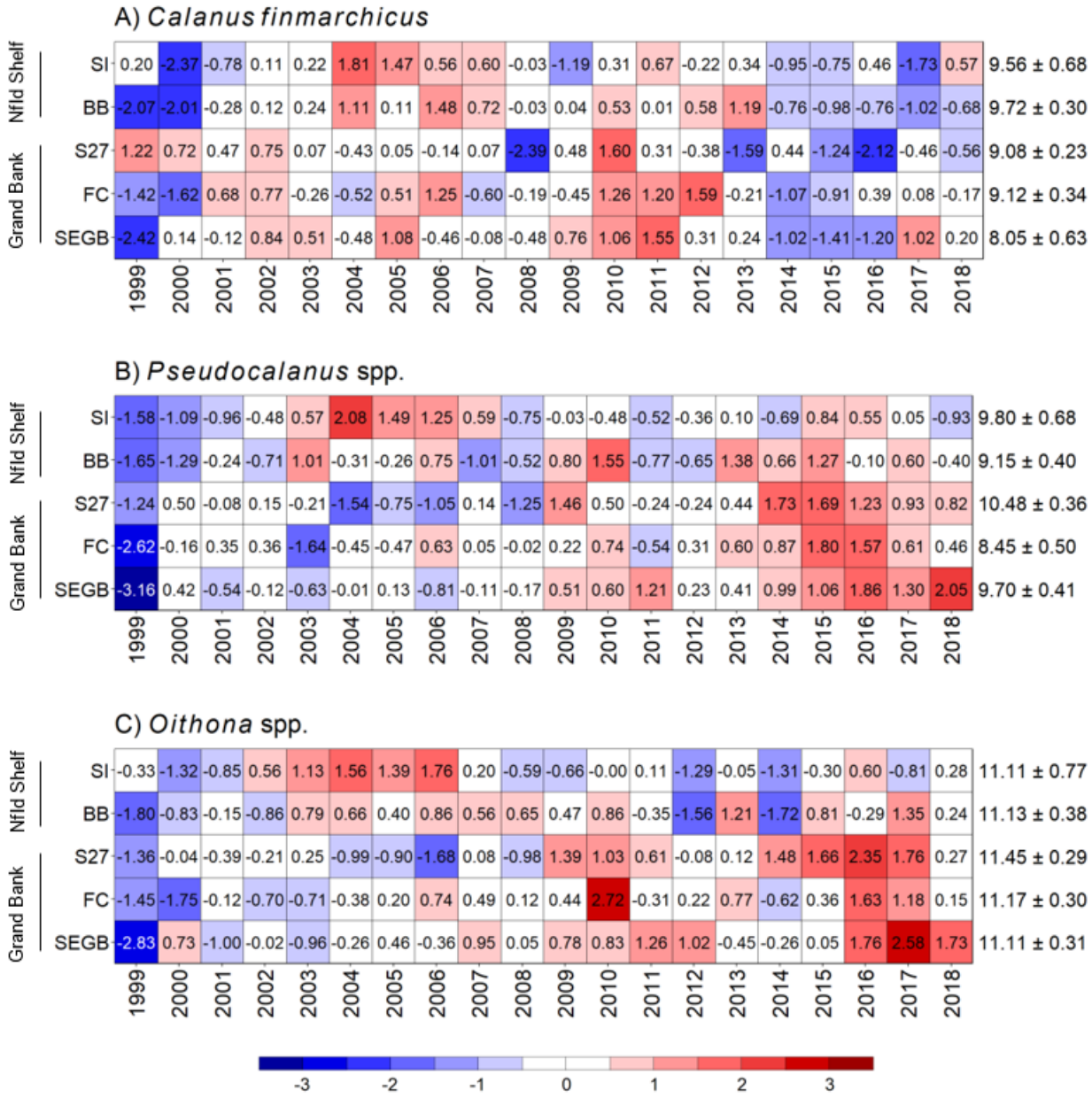

Figure 18. Annual anomaly scorecards for the abundance of large (A) and small (B, C) copepod taxa. Numbers in each cell are anomalies from the mean for 1999–2015 climatology in standard deviation units (mean [ln 1 + concentration in ind. m^{-2}] and SD listed at right). Red (blue) cells indicate higher (lower) abundance. White cells indicate near normal abundance. Sections are listed from north (top) to south (bottom). SI: Seal Island; BB: Bonavista Bay; S27: Station 27; FC: Flemish Cap; SEGB: Southeast Grand Bank. See Figure 1 for section geographical location.

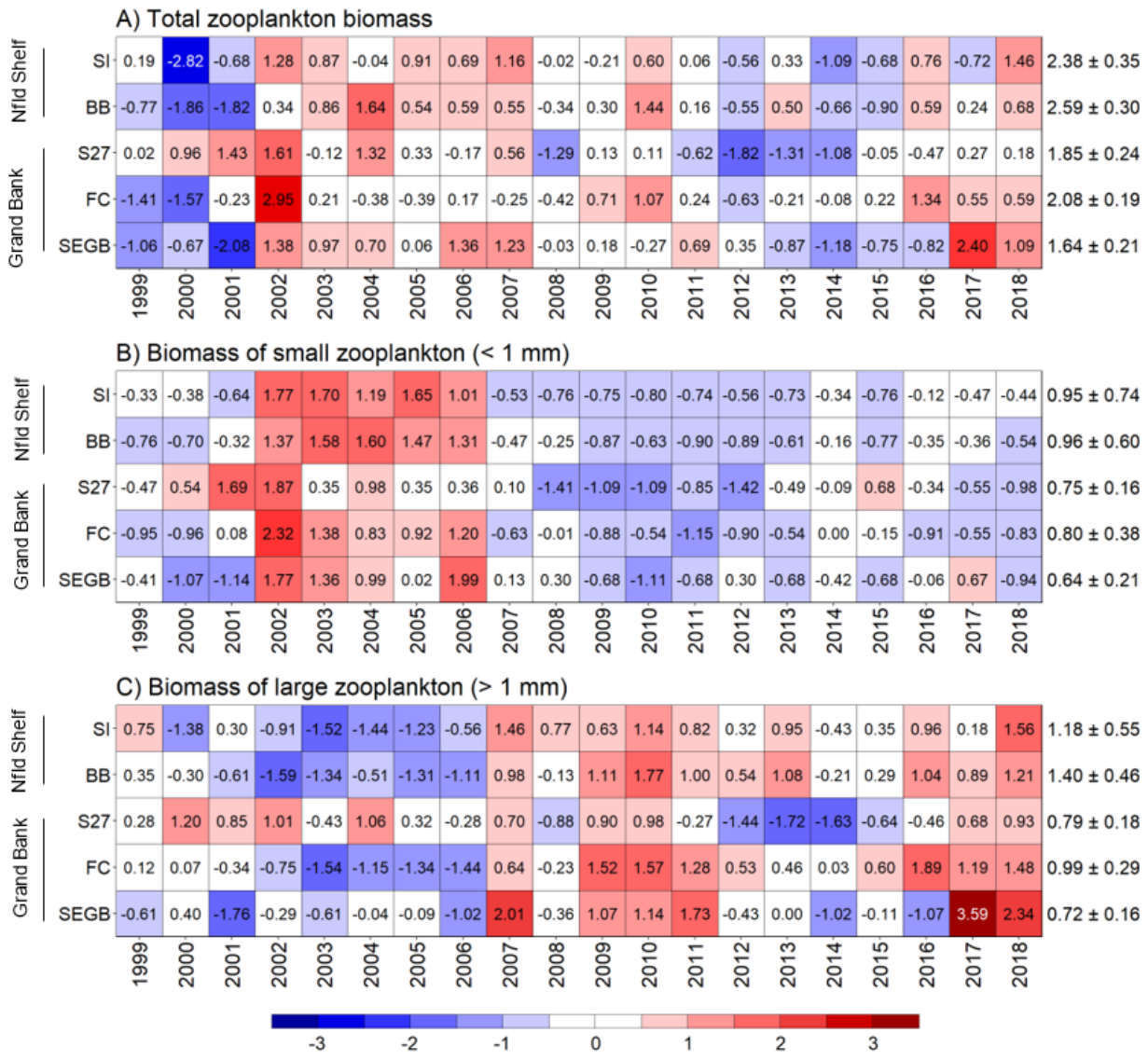

Figure 19. Annual anomaly scorecards for total zooplankton (A) and for the small (b) and large (C) size fractions. Numbers in each cell are anomalies from the mean for the 1999–2015 climatology in standard deviation units (mean [ln 1 + biomass in g m^{-2}] and SD listed at right). Red (blue) cells indicate higher (lower) than normal biomass. White cells indicate near normal biomass. Sections are listed from north (top) to south (bottom). SI: Seal Island; BB: Bonavista Bay; S27: Station 27; FC: Flemish Cap; SEGB: Southeast Grand Bank. See Figure 1 for section geographical location.

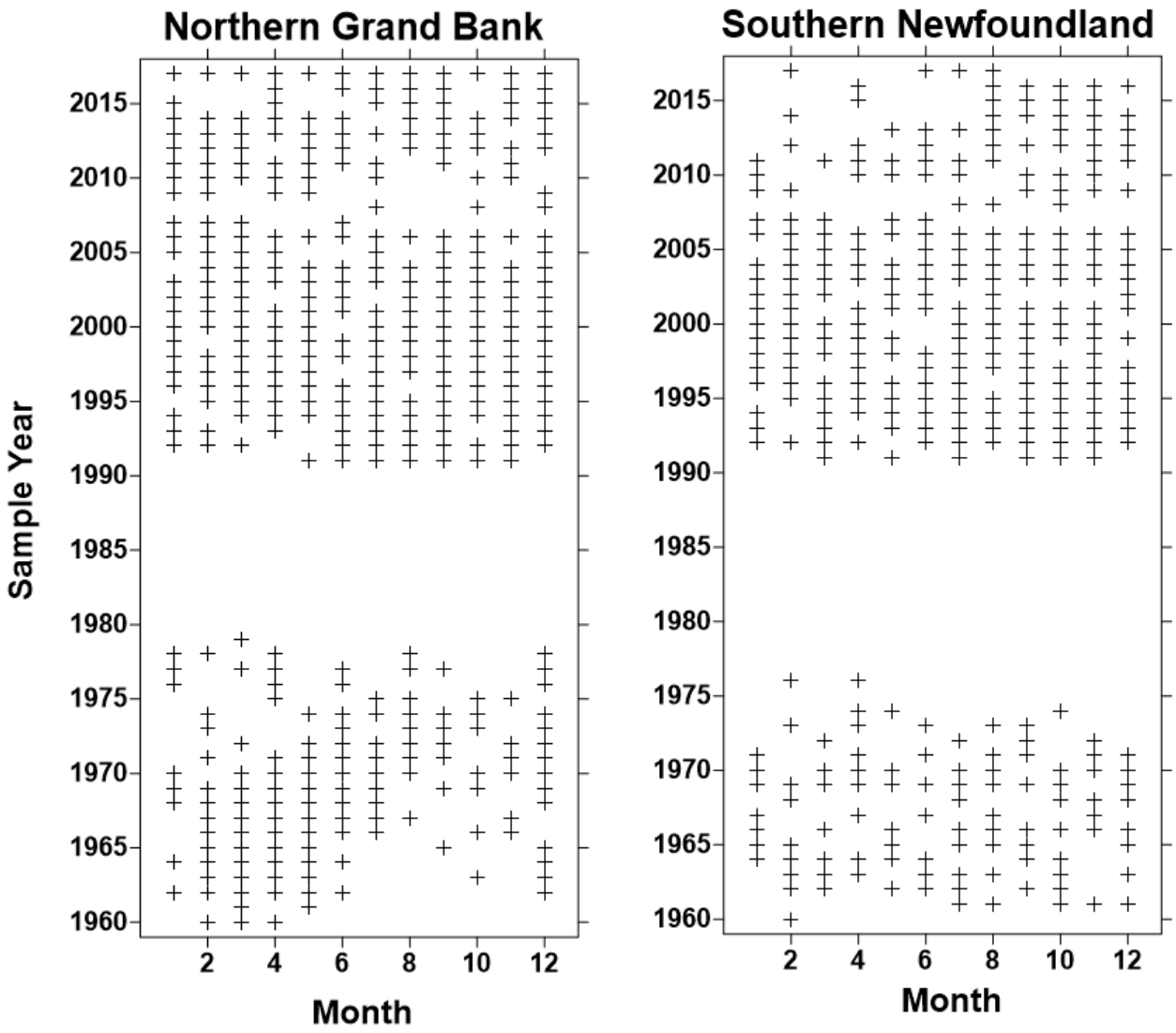

Figure 20. Monthly sampling frequency for the CPR on the northern Grand Bank (left panel) and southern Newfoundland (right panel). Note the large sampling gap starting in the mid-1970's until 1991.

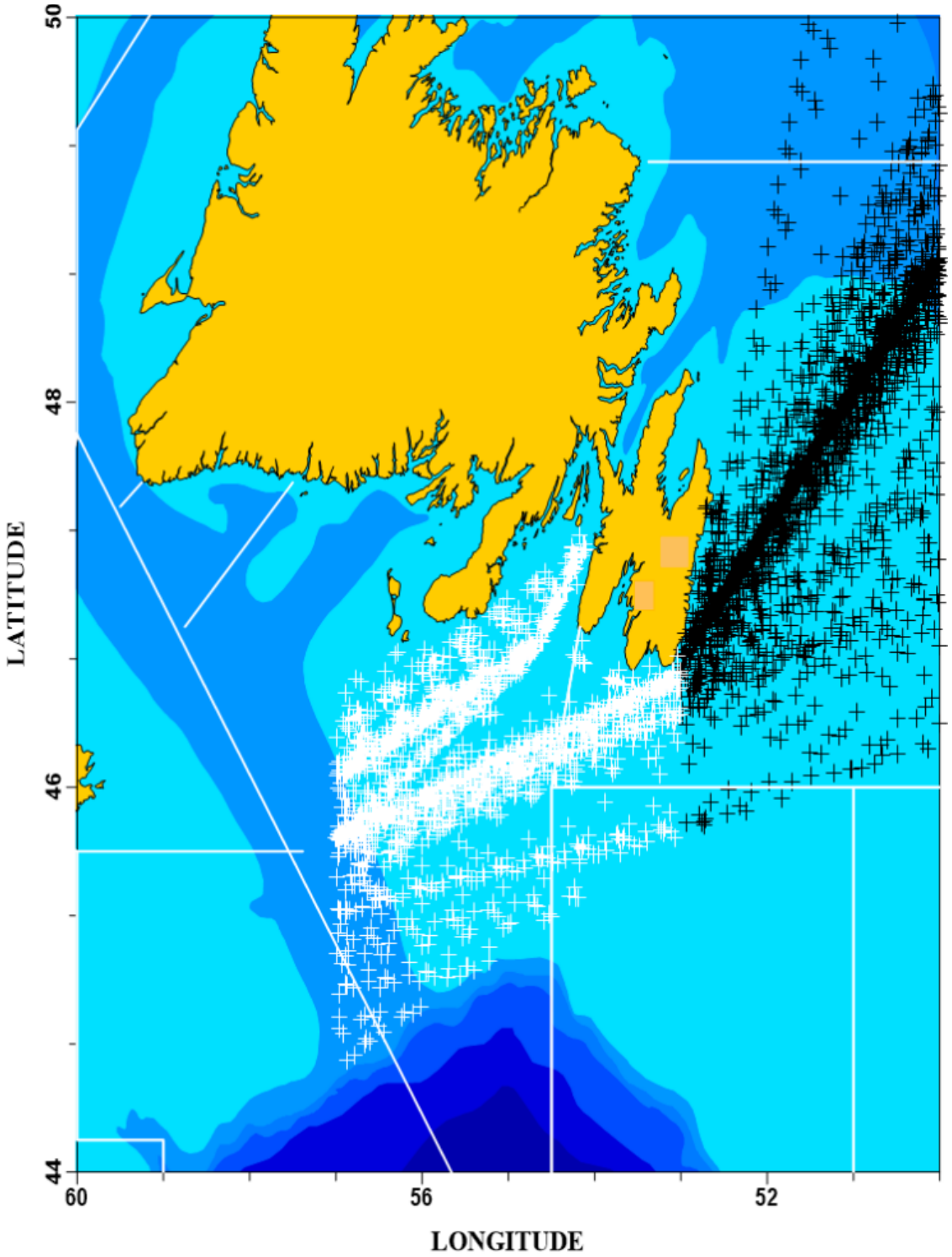

Figure 21. Commercial tow tracks and discrete stations of the CPR covering the continental shelf and slope waters during 1961–2017. Black (white) crosses indicate stations on the northern Grand Bank and southern Newfoundland.

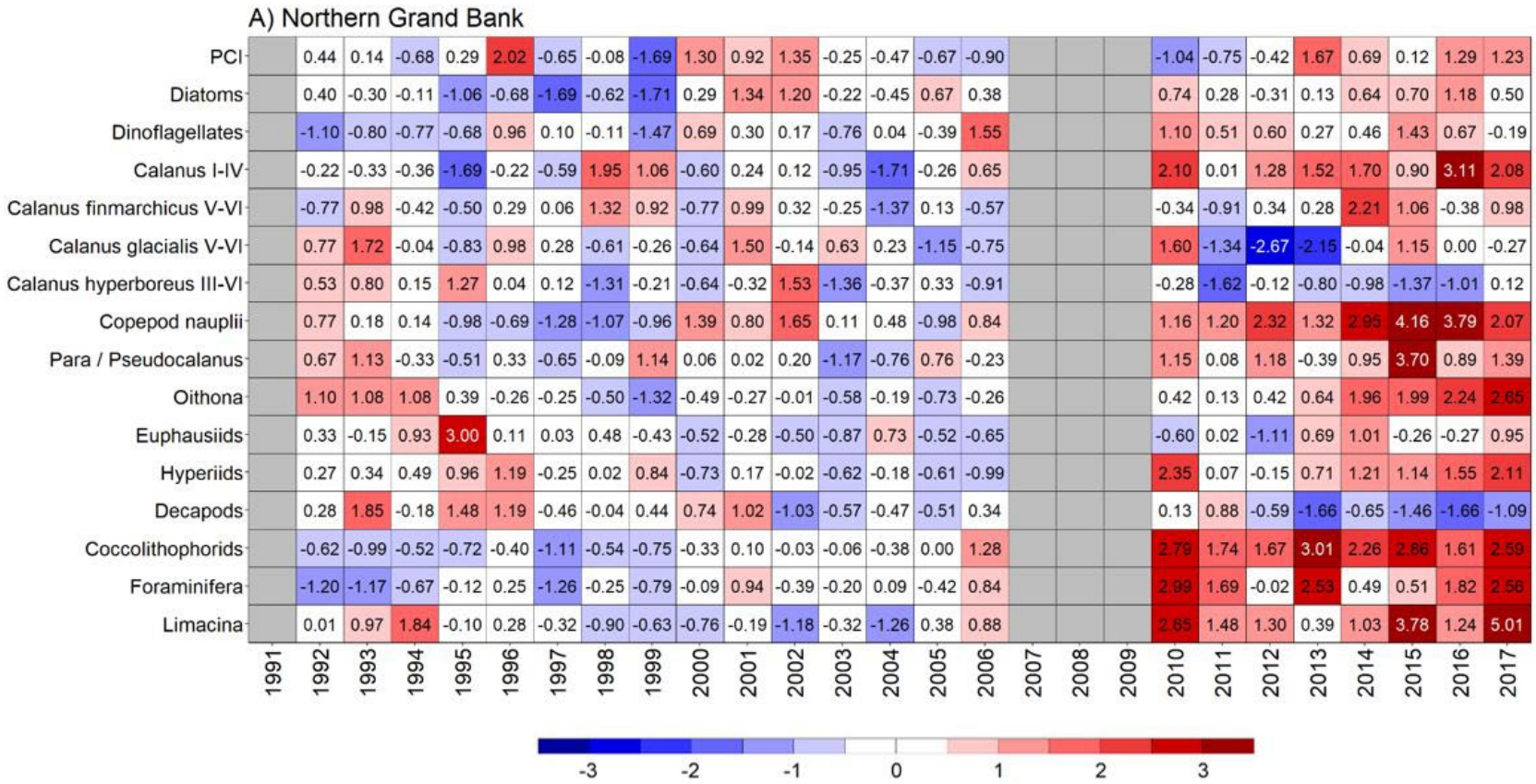

Figure 22. Annual anomaly scorecard for the relative abundances of phytoplankton and zooplankton taxa from the Continuous Plankton Recorder Survey on the northern Grand Bank (A) and southern Newfoundland (B) from 1991 to 2017. Numbers in each cell are anomalies from the mean for the reference period (1991–2010) in standard deviation (SD) units. Grey cells indicate years where sampling occurred in 8 or fewer months, or years with sampling gap of 3 or more consecutive months. Red (blue) cells indicate higher (lower) than normal values. White cells indicate near normal conditions (±0.5 SD). Acid sensitive taxa include coccolithophorids, foraminifera and the pteropod Limacina.

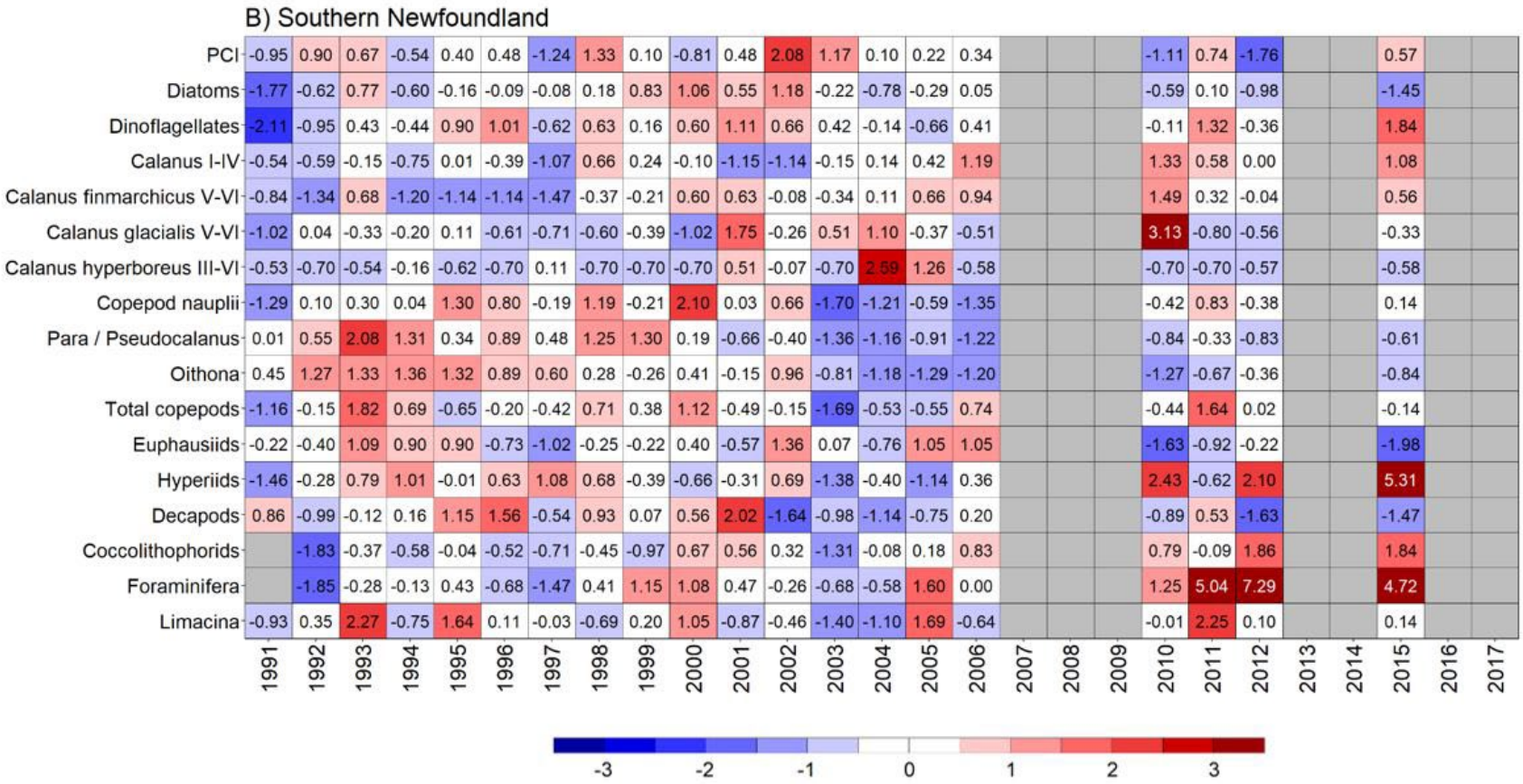

Figure 22 continued.

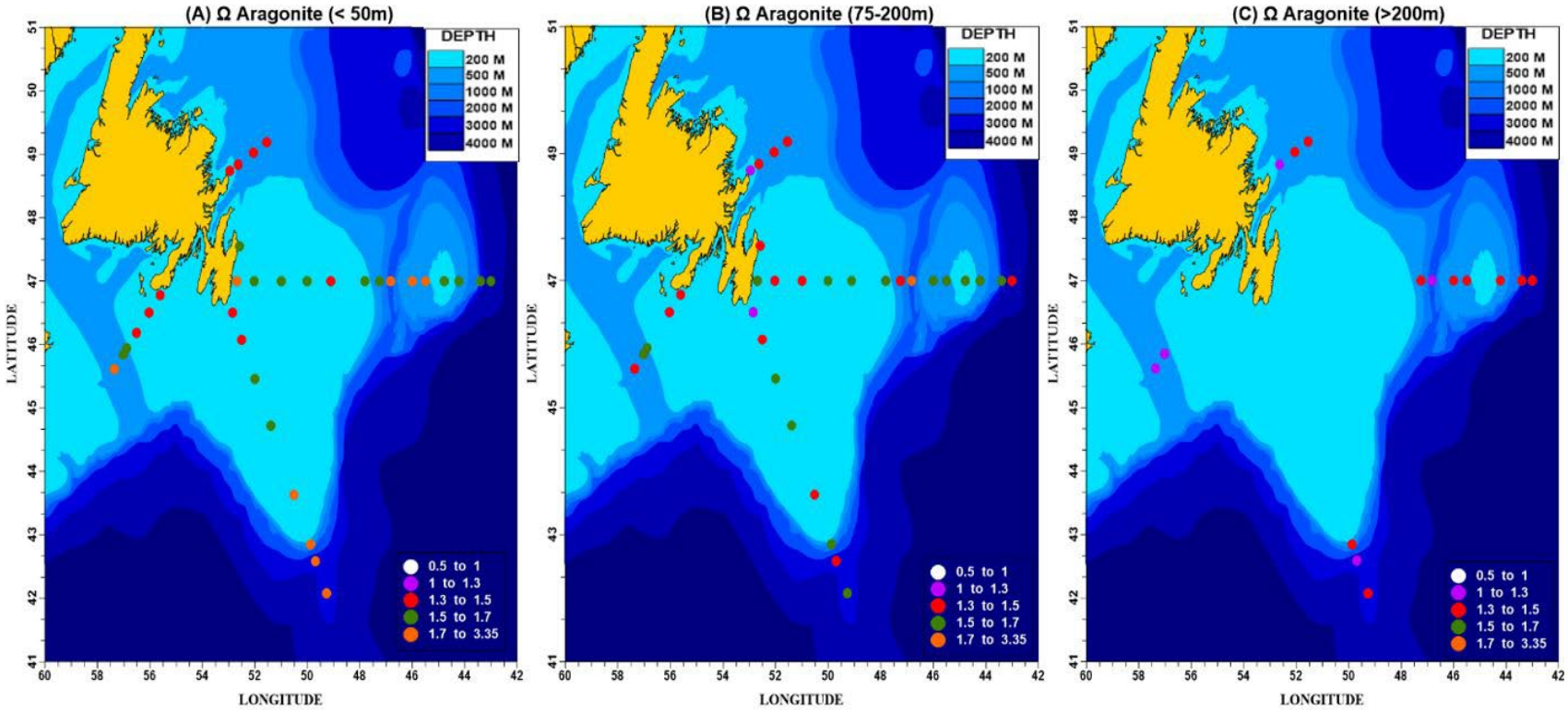

Figure 23. Saturation state of aragonite (upper panels) in (A) upper 50 m, (B) intermediate waters (75–200 m), and (C) >200 m (maximum depth 1,200 m) during the 2018 AZMP spring (March-April) missions. Corresponding ocean pH (total scale) conditions (bottom panels; D-F). Values of saturation state Omega (Ω) <1 indicate under-saturation while Ω >1 indicate conditions of over-saturation.

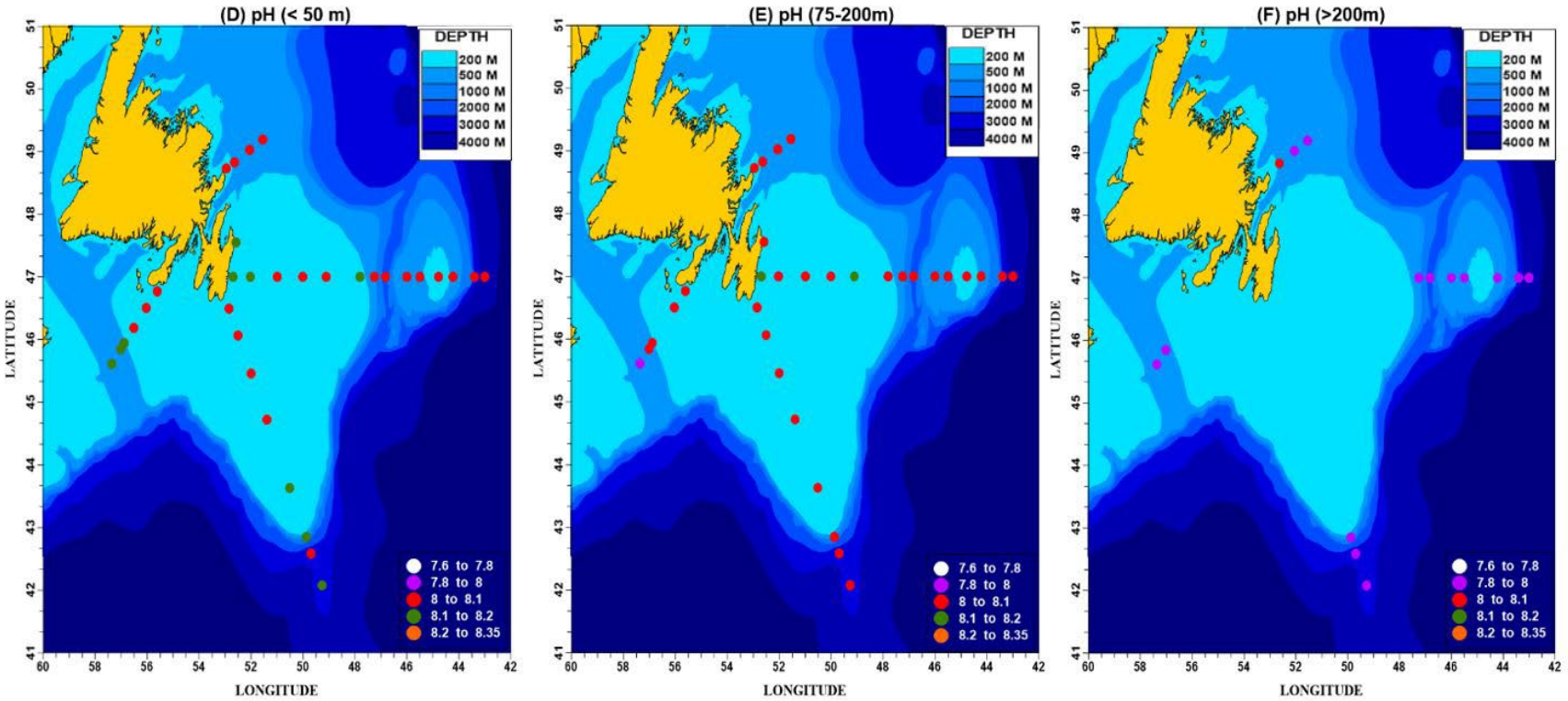

Figure 23 continued.

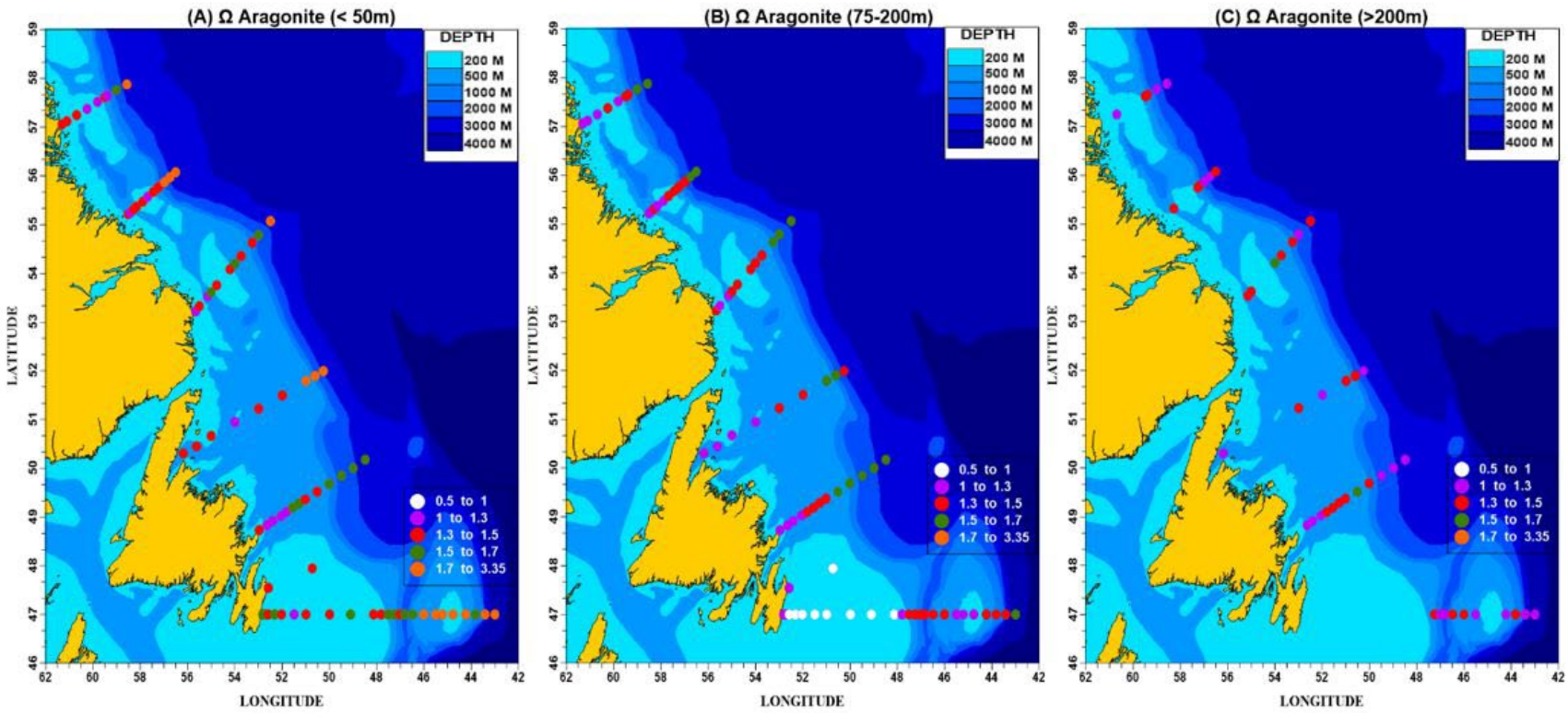

Figure 24. Saturation state of aragonite (upper panels) in (A) upper 50 m, (B) intermediate waters (75–200 m), and (C) >200 m (maximum depth 1,200 m) during the 2018 AZMP summer (July) missions. Corresponding ocean pH (total scale) conditions (bottom panels; D-F). Values of saturation state Omega (Ω) <1 indicate under-saturation while Ω >1 indicate conditions of over-saturation.

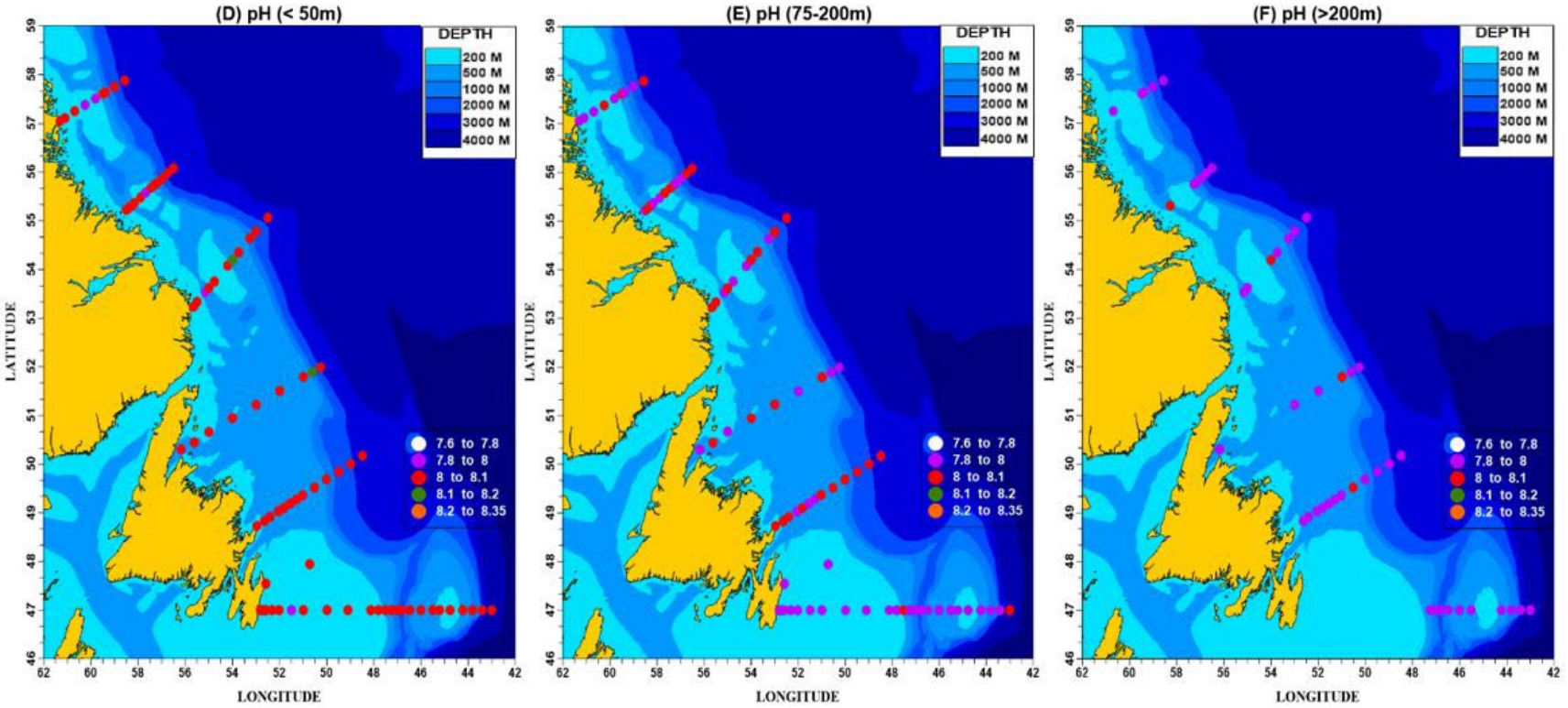

Figure 24 continued.

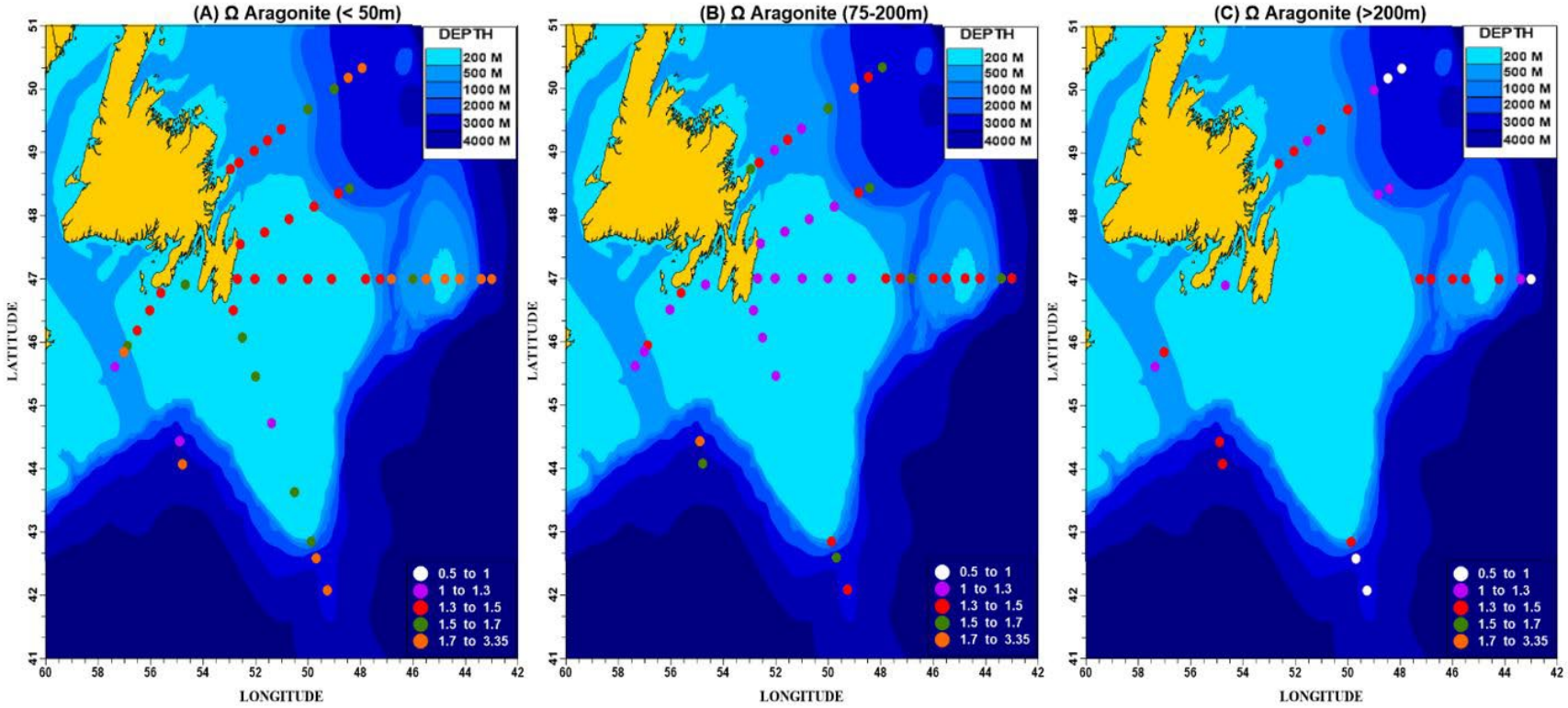

Figure 25. Saturation state of aragonite (upper panels) in (A) upper 50 m, (B) intermediate waters (75–200 m), and (C) >200 m (maximum depth 3,700 m) during the 2018 AZMP fall (Nov-Dec) missions. Corresponding ocean pH (total scale) conditions (bottom panels; D-F). Values of saturation state Omega (Ω) <1 indicate under-saturation while Ω >1 indicate conditions of over-saturation.

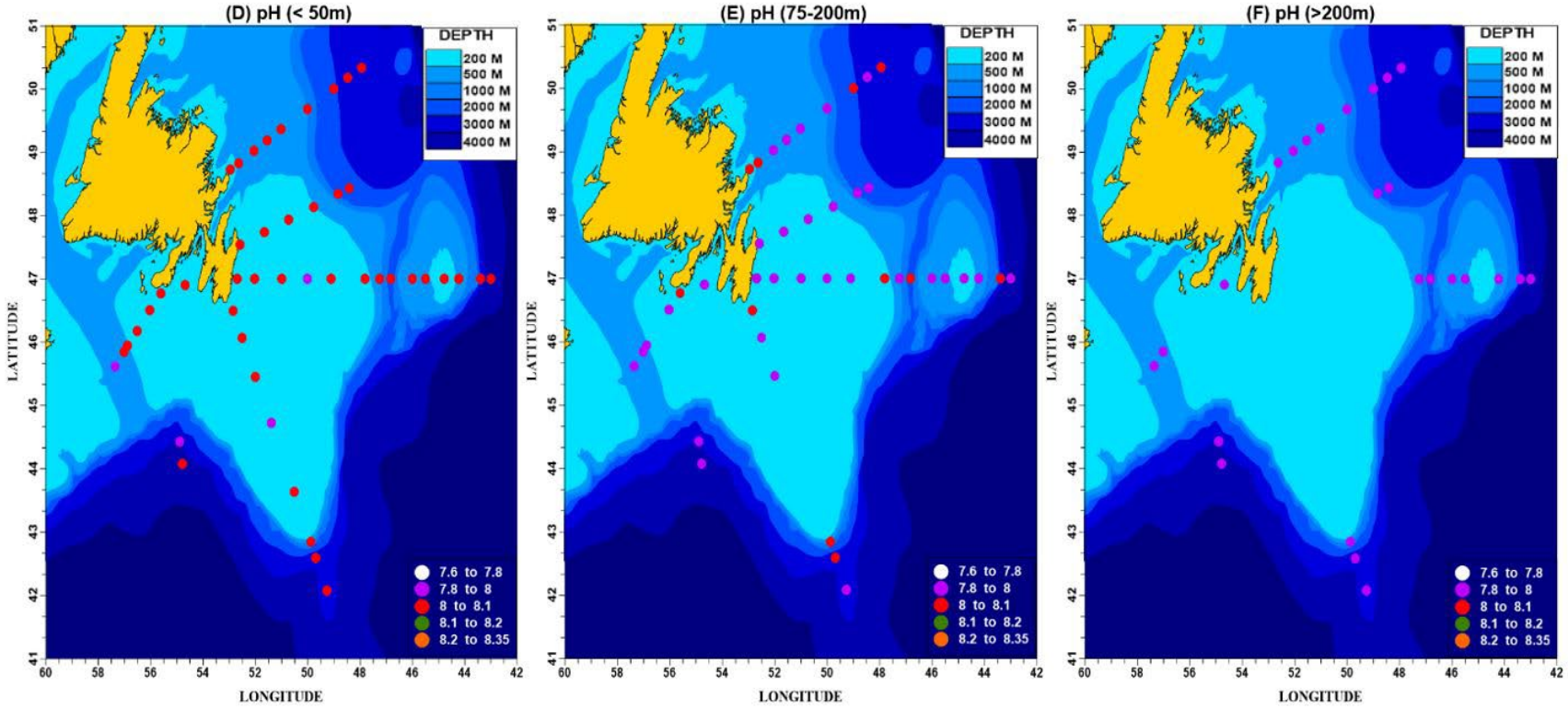

Figure 25 continued.

APPENDIX

APPENDIX 1. CORRECTED ZOOPLANKTON BIOMASS

Archiving errors in the DFO NL zooplankton database were discovered in 2019. Zooplankton biomass from samples collected between 2015 and 2018 at the high frequency sampling station (S27) and during seasonal surveys were not properly corrected to account for the split fraction of the subsamples used to quantify biomass. This led to an underestimation of the biomass during that period. In addition, a thorough review of the biomass database revealed that 205 biomass samples collected between 2013 and 2015 at S27 (n=3) and along the Seal Island (n=20), Bonavista Bay (n=52), Flemish Cap (n=98), and Southeast Grand Bank (n=32) had not been included in the database. The missing samples and the wrongly corrected biomass affected the climatological mean biomass values for the 1999–2015 reference period and, therefore, the biomass anomalies reported in the previous report by Maillet et al. (2019).

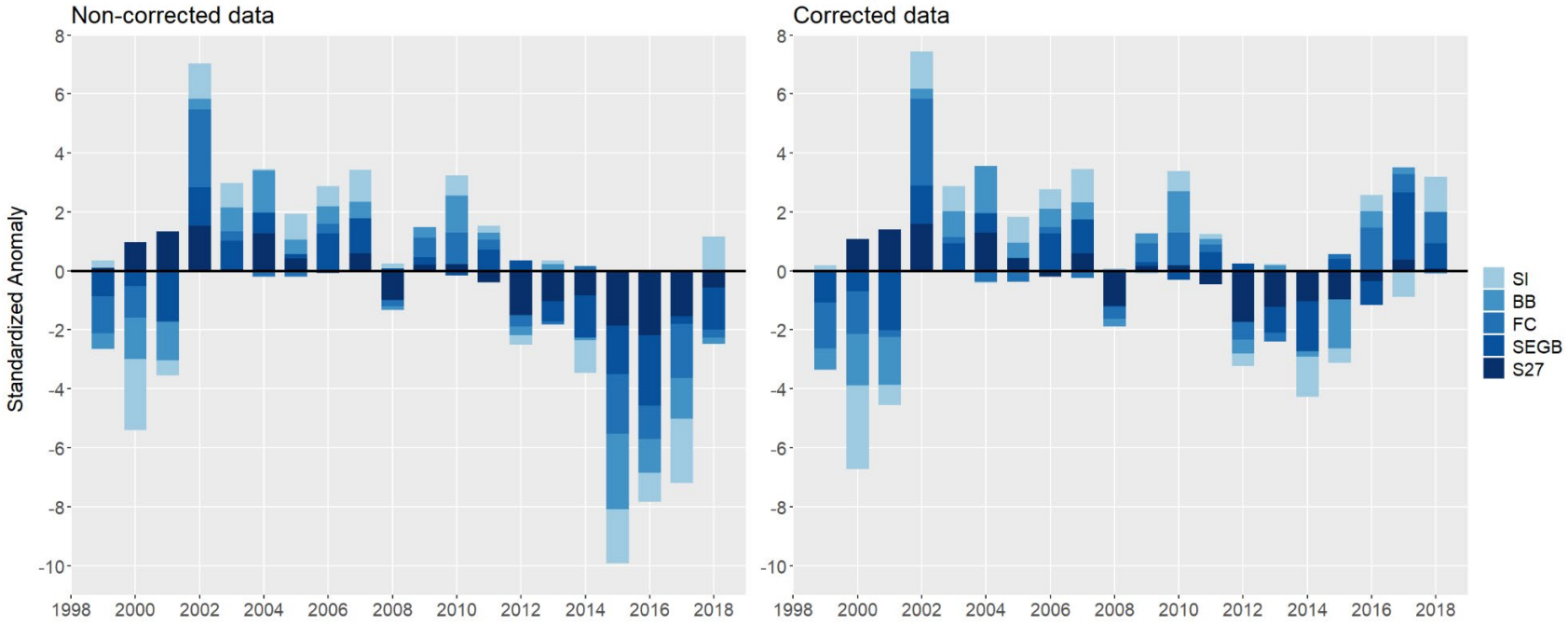

Figure A.1. Comparison of annual zooplankton anomalies between non-corrected (left panel) and corrected (right panel) biomass data for the coastal high frequency sampling station (S27) and the oceanographic sections (SI: Seal Island, BB: Bonavista Bay, FC: Flemish Cap, SEGB: Southeast Grand Bank). See Figure 1 for geographical location of the sampling station and sections.